Cell Reports

Article

Electrochemical coupling at the plasma membrane by mouse voltage-sensitive phosphatase requires association with basigin

Graphical abstract

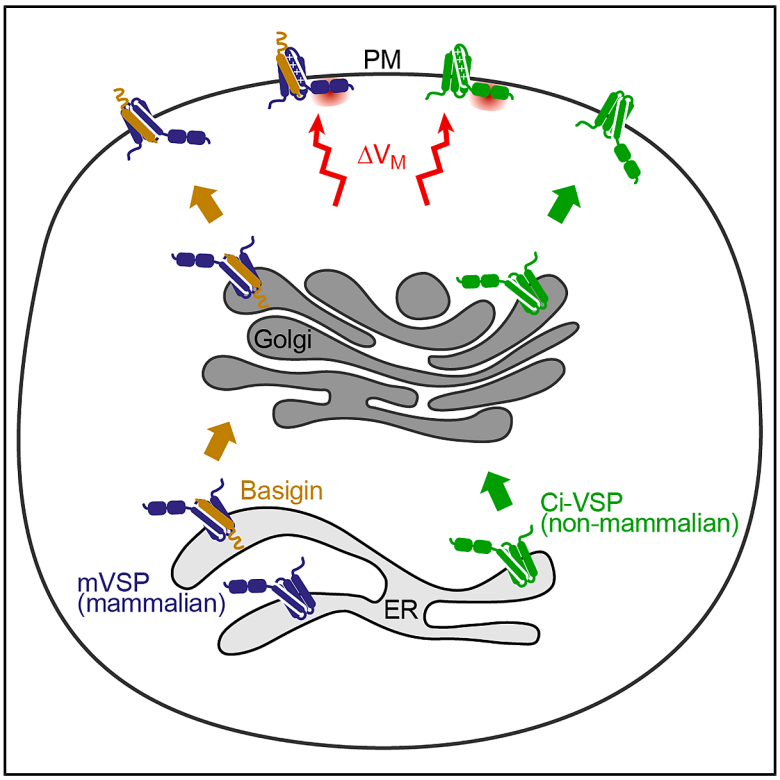

Authors

Imran G. Shaikh, Andrei Y. Kostritskii, Aparna Renigunta, ..., Jan-Philipp Machtens, Dominik Oliver, Vijay Renigunta

Correspondence

oliverd@staff.uni-marburg.de (D.O.), vijay@staff.uni-marburg.de (V.R.)

In brief

Shaikh et al. demonstrate that basigin binds to and controls trafficking of mouse voltage-sensitive lipid phosphatase (mVSP). Basigin promotes plasma membrane localization of mVSP, allowing for control of its activity by the membrane potential. Functional characterization of electrochemical coupling shows phosphoinositide phosphatase activity in a physiological voltage range.

Highlights

- Mouse voltage-sensitive phosphatase (mVSP) binds basigin
- Basigin interaction controls surface localization of mVSP
- Characterization of lipid phosphatase activity of a mammalian VSP
- mVSP is active at physiological membrane potentials

Shaikh et al., 2025, Cell Reports *44*, 116200
September 23, 2025
https://doi.org/10.1016/j.celrep.2025.116200

CellPress

Cell Reports

CellPress
OPEN ACCESS

Article

Electrochemical coupling at the plasma membrane by mouse voltage-sensitive phosphatase requires association with basigin

Imran G. Shaikh,[1] Andrei Y. Kostritskii,[2] Aparna Renigunta,[3] Julia Jeschke,[1] Christian R. Halaszovich,[1] Wencai Zhao,[1] Marc Geissler,[1] Sudhanshu Bhushan,[4] Stefanie Weber,[3] Andreas Meinhardt,[4] Jan-Philipp Machtens,[2,5] Dominik Oliver,[1,6,7,*] and Vijay Renigunta[1,*]

[1]Institute for Physiology and Pathophysiology, Philipps University Marburg, 35037 Marburg, Germany
[2]Institute of Biological Information Processing (IBI-1), Molekular- und Zellphysiologie, Forschungszentrum Jülich, 52428 Jülich, Germany
[3]Department of Pediatrics, University Hospital Giessen and Marburg, Philipps University Marburg, 35043 Marburg, Germany
[4]Institute of Anatomy and Cell Biology, Unit of Reproductive Biology, Justus Liebig University Giessen, 35392 Giessen, Germany
[5]Institute of Neurophysiology, Hannover Medical School, 30625 Hannover, Germany
[6]Center for Mind, Brain and Behavior (CMBB), Universities of Marburg and Giessen, Marburg, Germany
[7]Lead contact
*Correspondence: oliverd@staff.uni-marburg.de (D.O.), vijay@staff.uni-marburg.de (V.R.)
https://doi.org/10.1016/j.celrep.2025.116200

SUMMARY

Voltage-sensitive phosphatases (VSPs) are unique enzymes that mediate electrochemical coupling by converting phosphoinositides in response to membrane depolarization. In mammals, VSPs are involved in regulating sperm motility. The basic functionality of mammalian VSPs has remained enigmatic, as retention to intracellular compartments precluded functional analysis. Here, a membrane yeast two-hybrid assay identifies basigin as an accessory subunit of mouse VSP (mVSP). Co-expression with basigin or its homologs induced trafficking of mVSP from the endoplasmic reticulum to the plasma membrane. Mutational analysis and structural predictions by AlphaFold-Multimer showed that the functional effect on mVSP requires interaction of the transmembrane region of basigin with the voltage sensor domain of mVSP. Basigin-mediated surface localization allowed for functional analysis, revealing that mVSP acts as a voltage-activated 5-phosphatase against $PI(4,5)P_2$ and $PI(3,4,5)P_3$ with a more negative activation range compared to non-mammalian VSPs.

INTRODUCTION

Voltage-sensitive phosphatases (VSPs) are unique phosphoinositide (PI)-modifying enzymes considered to control PI-mediated signal transduction pathways.[1–3] VSPs consist of a C-terminal intracellular phosphatase domain (PD) coupled to an N-terminal transmembrane voltage sensor domain (VSD), structurally homologous to the VSD of voltage-gated ion channels.[4,5] According to functional studies, predominantly on the non-vertebrate VSP from the sea squirt *Ciona intestinalis*, this modular organization underlies the regulation of the enzymatic domain by membrane potential. Thus, the phosphatase is inactive at the negative membrane potential that is typical of most cells under resting conditions, whereas depolarization triggers phosphatase activity.[1,6] The PD is homologous to the lipid phosphatase and tumor suppressor PTEN,[7,8] a 3-phosphatase that inhibits phosphatidylinositol 3-kinase signaling through dephosphorylation of $PI(3,4,5)P_3$. In contrast to PTEN, however, VSPs dephosphorylate both $PI(4,5)P_2$, the main PI of the eukaryotic plasma membrane (PM), and $PI(3,4,5)P_3$. The latter activity generates another PI, $PI(3,4)P_2$.[6,9] Indeed, when activated by depolarization, VSPs can rapidly and strongly deplete $PI(4,5)P_2$ and $PI(3,4,5)P_3$ while simultaneously increasing $PI(3,4)P_2$ levels in the PM.[6,9] Of note, these three PIs are important regulators of cellular functions, including Akt signaling, actin dynamics, and membrane remodeling, and the activity of membrane proteins such as transporters and ion channels.[2] Accordingly, VSP proteins have been widely used as tools to study the role of PIs in regulating cellular mechanisms.[10–13]

In spite of extensive work on molecular mechanisms of model VSPs, mostly *C. intestinalis* VSP (Ci-VSP), surprisingly little is known about their biological functions. VSPs seem to be a general feature of chordates, from sea squirts up to vertebrates, including mammals.[1,14–20] Expression patterns of VSP proteins appear to vary between species[16,17,21,22] and are incompletely understood, likely due to the lack of high-quality antibodies. However, a consistent finding is VSP expression in the testes, where it localizes to sperm or sperm precursor cells.[23,24] A recent study demonstrated impaired sperm motility in mice deficient for VSP, which was attributed to the disruption of polarized distribution of $PI(4,5)P_2$ along the sperm flagellum.[24]

Nevertheless, full elucidation of the proposed mechanism and, more generally, understanding of VSP biology in mammals are

impeded by the lack of knowledge of the basic functionality of mammalian VSPs. In heterologous expression systems, mammalian VSPs (e.g., from mouse and humans [mVSP and hVSP1, respectively]) are exclusively localized to intracellular compartments, mainly the endoplasmic reticulum (ER).[9,25] Consequently, it has been impossible to study enzymatic activity and voltage sensitivity; so far, $PI(4,5)P_2$ phosphatase activity of the PD was merely inferred from chimeric constructs between non-mammalian and mammalian VSP.[9,25] Moreover, the subcellular distribution of native VSPs in their natural cellular environment has not been reported so far.

Many proteins targeted to the PM rely on accessory or ancillary proteins for their trafficking.[26–31] We screened for mouse VSP interaction proteins using a membrane yeast two-hybrid assay. This unbiased approach identified basigin (BSG), also known as CD147, as a candidate interaction partner of mVSP. Basigin is known to be expressed in mammalian sperm, where it is essential for regular spermatogenesis and sperm motility.[32,33] Strikingly, co-expression of mVSP with basigin induced robust PM localization of mVSP. Biochemical and mutational analysis showed the direct interaction of both proteins via their transmembrane (TM) domains, revealing basigin as an essential accessory subunit of PM-targeted mVSP. Surface localization allowed for functional examination, showing that mammalian VSP is a *bona fide* VSP that dephosphorylates $PI(4,5)P_2$ and PIP_3 when activated by depolarization of the membrane potential.

These findings suggest that, in the mammalian lineage, a second layer of regulation of VSP activity evolved; in addition to acute regulation by membrane potential, the interaction with basigin controls subcellular trafficking of VSP to the PM, facilitating electrochemical control of PI signaling.

RESULTS

Identification of basigin as an mVSP-interacting protein

To identify proteins that interact with mVSP, we performed a yeast two-hybrid screen using the split-ubiquitin variant that enables the use of full-length integral membrane proteins as baits for interactions with integral membrane proteins and membrane-associated proteins (Figure 1A). Given the reported expression of mVSP in the brain,[25] we screened a mouse brain cDNA library. Briefly, the C-terminal half of ubiquitin, along with an artificial transcription factor, was fused to the N terminus of mVSP. A control assay using positive and negative control prey vectors was performed to verify the functionality of the bait vector. The positive controls showed that the bait proteins were robustly expressed in the yeast strain (Figures S1A–S1D). Screening with brain cDNA-encoded proteins fused to the N-terminal half of ubiquitin resulted in the identification of several interaction candidates. One of these proteins was the transmembrane glycoprotein basigin 2, also known as CD147. The protein has two immunoglobulin (Ig)-like domains (D2 and D1), a transmembrane region, and an intracellular C-terminal region (Figure 2A). In a specific yeast two-hybrid assay using mVSP as the bait and basigin as the prey, the robust interaction of mVSP with basigin was confirmed (Figure 1B).

To further scrutinize the putative interaction, we performed co-immunoprecipitation studies using cell lysates from HeLa cells expressing ^{GFP}mVSP + basigin^{FLAG} constructs in one set of experiments or, vice versa, mVSP$^{3\times FLAG}$ + basigin^{GFP} constructs in another set of experiments (Figures 1C and 1D). GFP-tagged mVSP protein was immunoprecipitated by anti-FLAG antibodies from HeLa cell lysates expressing ^{GFP}mVSP and basigin^{FLAG} (Figure 1C). Conversely, we detected GFP-tagged basigin protein in the anti-FLAG immunoprecipitates of HeLa cells expressing mVSP$^{3\times FLAG}$ and basigin^{GFP} proteins (Figure 1D). Negative controls involved HeLa cell lysates expressing GFP instead of GFP fusion constructs (Figures 1C and 1D), and lysates obtained from fusion constructs precipitated using beads coated with unrelated IgG antibodies (Figures S1E and S1F). Taken together, yeast two-hybrid (Y2H) results and the reciprocal co-immunoprecipitation of mVSP and basigin indicate a *bona fide* protein-protein interaction between the two membrane proteins.

Basigin regulates localization of mVSP to the cell surface

We next examined the interaction of basigin with mVSP in cells. GFP-tagged mVSP transiently expressed in HeLa cells localized to intracellular compartments, with a major fraction of the protein associated with a perinuclear compartment (Figures 2A and 2B). In contrast, basigin, visualized by RFP fusion, was robustly localized to the cell surface, yielding peaks of fluorescence intensity at the cell margins in plots of fluorescence intensity profiles across the cell (Figures 2A and 2C). A similar distribution of the proteins was observed in Chinese hamster ovary (CHO) and HEK293 cells (Figure S2). Co-expression of both proteins, however, resulted in a high degree of spatial co-localization, resulting from pronounced localization of mVSP at the cell surface rather than intracellular compartments in HeLa cells (Figure 2D), as well as in CHO and HEK293 cells (Figure S2). This shift in localization indicated basigin-dependent trafficking of mVSP to the PM, as shown by co-localization of mVSP with a membrane marker PLCδ1-PH-RFP, in the presence of myc-tagged basigin (Figures 2E and 2F). To corroborate these findings in a quantitative manner, the PM/cytoplasmic ratio of mVSP was estimated, making use of localization of RFP-tagged basigin to define the position of the PM (Figure S3). In the absence of co-expressed basigin, the PM/cytoplasmic ratio of mVSP-GFP was <1. However, when myc-basigin was co-expressed, the ratio was strongly increased (to >2), providing evidence of robust localization of mVSP at the PM (Figure 2G). We additionally used antibody labeling of a hemagglutinin (HA) epitope introduced into the small extracellular domain of the VSD of mVSP (Figure 2H). In non-permeabilized cells, the anti-HA antibody labeled only cells co-expressing myc-basigin (Figure 2I, right) but not cells expressing mVSP-HA alone (Figure 2I, left), confirming that basigin is required for trafficking mVSP to the PM.

Basigin is a member of a small family of three homologous proteins that also includes neuroplastin and embigin.[34–36] We wondered whether neuroplastin and embigin were equally capable of inducing PM localization of mVSP protein to the PM. As shown in Figure 3, co-expression of either basigin family member in HeLa cells resulted in pronounced localization of

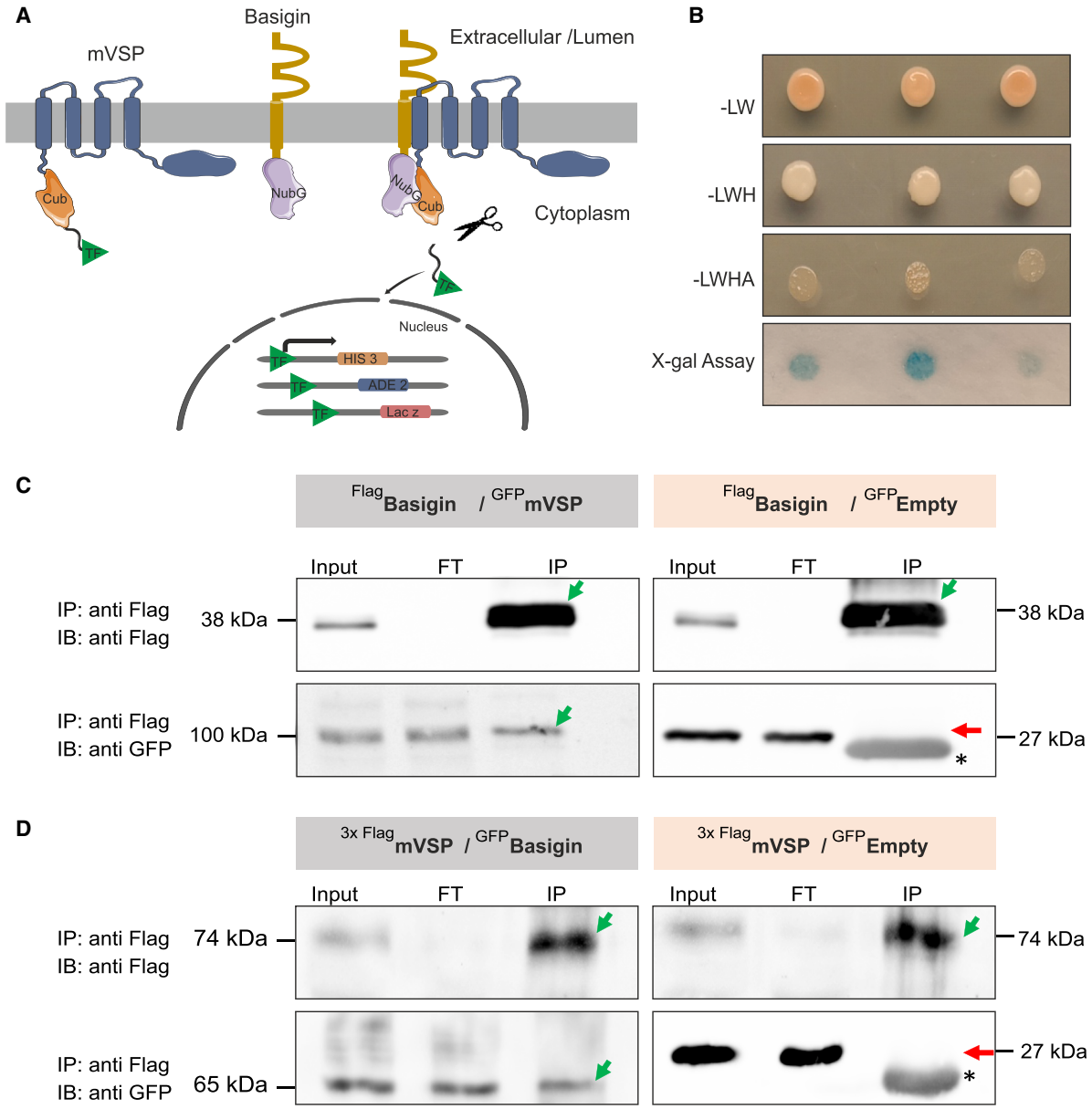

Figure 1. VSP interacts with basigin

(A) Membrane Y2H constructs used in this study. mVSP, fused to the C-terminal half of ubiquitin (Cub) along with an artificial transcription factor (TF) and a downstream reporter cassette, was used as bait, and basigin fused to the N-terminal half of ubiquitin (Nub) was used as prey.

(B) Y2H assay showing interaction between mVSP and basigin. Growth on −LW plates confirms co-transformation with bait and prey plasmids. Growth on −LWH plates indicates activation of the HIS3 reporter gene, while growth on −LWHA indicates stronger interaction via activation of both HIS3 and ADE2. β-galactosidase activity (blue) serves as an additional confirmation of interaction through lacZ reporter expression.

(C) CoIP of GFP-tagged VSP and FLAG-tagged basigin expressed in HeLa cells.

(D) CoIP of 3× FLAG-tagged VSP and GFP-tagged basigin expressed in HeLa cells. The complex containing VSP and basigin was precipitated from cell lysate using anti-FLAG antibody M2-conjugated agarose beads, and a western blot of the precipitate was probed with FLAG and GFP antibodies; the cell lysate (input) was used as a positive control. CoIP performed with GFP alone was used as a negative control (right).

Note that the two bands detected in the immunoprecipitate (C and D, marked with an asterisk) are not due to GFP but to immunoglobulins from the beads, detected only by the secondary antibody. Schematics were generated using Servier Medical Art, licensed under a Creative Commons Attribution 3.0 Unported License (https://creativecommons.org/licenses/by/3.0/).

mVSP to the PM. According to the PM/cytoplasmic ratio of mVSP-GFP, embigin was somewhat less efficient in promoting PM localization than basigin (Figure 3D). Taken together, these results indicate that basigin or its homologs are required to ensure localization of a mammalian VSP to the PM, independent of the cell type probed.

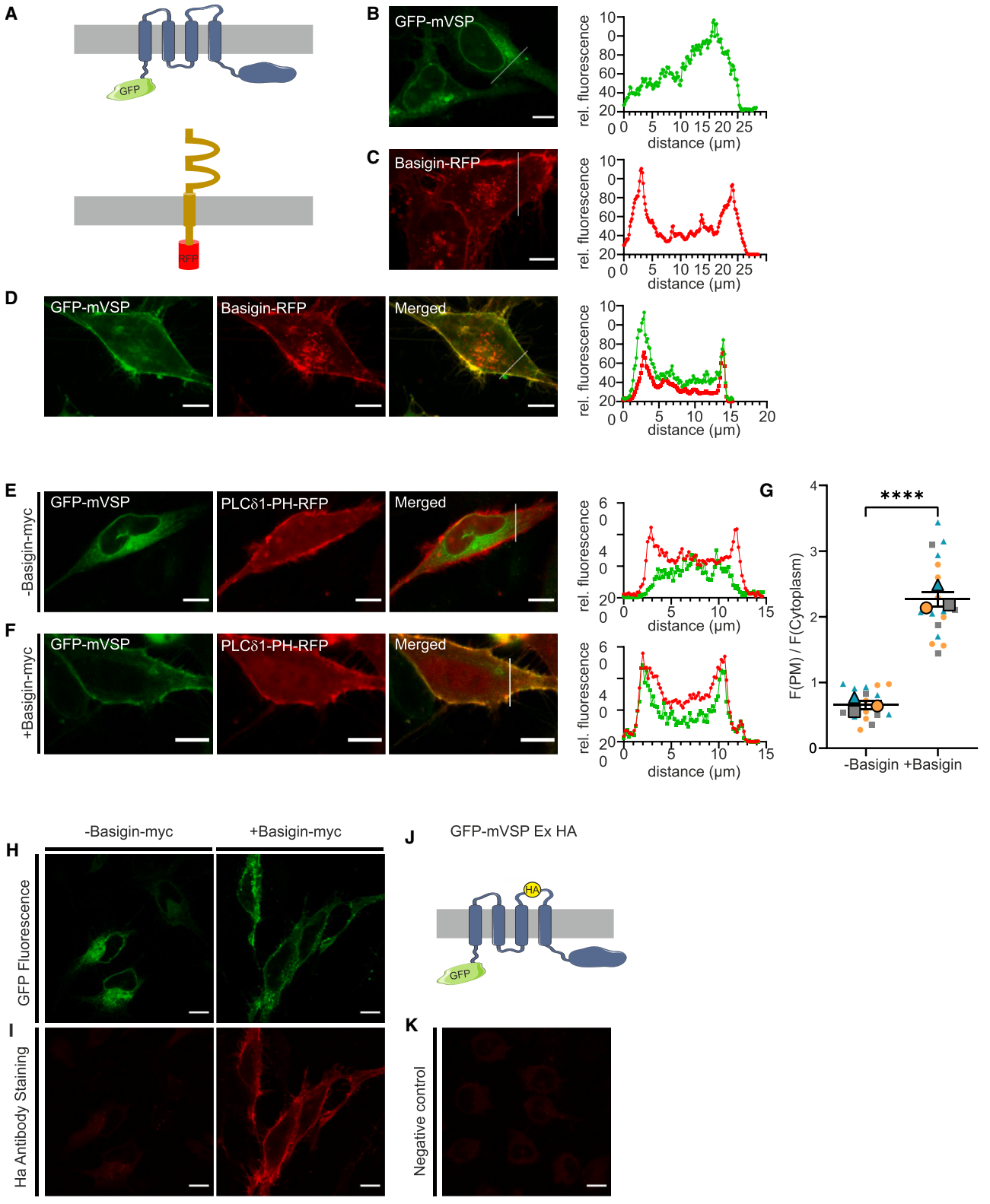

(legend on next page)

Association with basigin mediates escape from ER retention

The emergence of mVSP at the PM suggests that basigin (and its homologs) orchestrate protein trafficking of mammalian VSP. In order to identify the trafficking steps influenced by basigin, we sought to define the cellular compartments occupied by mVSP in the absence and presence of basigin. To this end, we analyzed co-localization with organelle markers along the secretory pathway. Without co-expression of basigin, cellular localization of mVSP-GFP largely coincided with the ER marker pDsRed2-ER (KDEL) and, to a lesser extent, with the Golgi marker galT-DsRed but not with the PM marker Lyn11-RFP (Figure 4A). Figure 4B shows that co-expression with basigin reduced overlap with the ER and Golgi markers, as a large fraction of the protein now appeared at the cell surface, where it precisely co-localized with Lyn11, as already shown above with a distinct PM marker, PLCδ1-PH (Figure 2F).

These observations suggested that mVSP is retained in the ER and Golgi, which is overcome by the presence of basigin. Nevertheless, we also considered that intracellular localization may reflect protein instability or misfolding. To address this possibility, we examined a possible association of mVSP with lysosomes, compartments involved in the degradation of misfolded proteins.[37,38] Co-expression of mVSP with the lysosomal marker LysoTracker Red revealed minor co-localization with lysosomes (Figures 4A and 4B, bottom). However, co-expression of basigin did not substantially alter lysosomal co-localization, indicating that inefficient targeting of mVSP to the PM is not caused by misfolding or protein instability.

Basigin-dependent forward trafficking (from the ER) might result from two distinct mechanisms. We considered that the presence of basigin at the ER might relieve retention of mVSP by influencing the sorting/trafficking machinery of the ER independent of its interaction with mVSP. Such a mechanism might seem plausible, given the similar effect of basigin family members on trafficking of other, structurally unrelated membrane proteins, monocarboxylate transporters (MCTs) and PM Ca^{2+} ATPases (PMCAs).[39,40] Alternatively, the interaction of mVSP with the trafficking machinery could be altered by binding of mVSP to basigin. Our finding of a protein-protein interaction between basigin and mVSP argues in favor of the latter mechanism. To distinguish between both possibilities, we devised an experiment where basigin was equipped with a strong ER retention motif ($basigin_{ERret}$; Figure 4C), analogous to a strategy implemented previously to address neuroplastin's impact on PMCA.[39] In contrast to wild-type basigin, $basigin_{ERret}$ was completely localized to intracellular compartments in a pattern consistent with residence in the ER (Figure 4D). When co-expressed with $basigin_{ERret}$, mVSP was completely retained with the same ER-like distribution and closely co-localized with the basigin construct (Figure 4E). Likewise, co-expression of mVSP with an analogous ER-retained neuroplastin construct[39] or with an ER-retained embigin construct resulted in retention of mVSP in an ER pattern (Figure S4). These findings indicate that the mere presence of basigin in the ER compartment is not sufficient to relieve ER retention of mVSP. Furthermore, the data provide evidence supporting interaction of both proteins at the level of the ER. We conclude that mVSP associates with basigin (or its homologs) at the ER and that formation of this complex allows mVSP to escape from ER retention, allowing forward trafficking to the PM.

While the mechanisms of ER retention and its release by basigin binding remain to be addressed at the mechanistic level, we note that basigin-dependent forward trafficking to the PM is a comparatively slow process. Thus, 24 h after co-transfection with basigin, mVSP was mostly localized to intracellular compartments, whereas pronounced PM localization was only observed after 48 h of incubation (Figures S5C and S5D). Notably, basigin alone typically reaches the PM within 24 h. However, when co-expressed with mVSP, its surface trafficking was also delayed, consistent with co-trafficking of both proteins as a complex (Figure S5). For comparison, the non-mammalian Ci-VSP, which neither experiences ER retention nor requires interaction with basigin for PM localization, achieved PM localization within 24 h (HeLa cells; Figures S5E and S5F).

Mapping the interaction interface between mVSP and basigin

The conserved interaction of all three basigin homologs with mVSP suggested a conserved protein interface mediating the interaction of both proteins. To identify the domains involved, we generated basigin truncation mutants lacking either the extracellular N-terminal Ig domains or the intracellular C terminus (Figures 5A–5D). These constructs retained their PM localization when expressed in HeLa cells (Figures S6A–S6D). Likewise, the potential of truncated basigin constructs to mediate membrane localization of co-expressed mVSP was unimpaired (Figures 5A–5D and 5I). Therefore, the interaction with mVSP and the control of mVSP trafficking do not require

Figure 2. mVSP is translocated to the surface of the membrane with the help of basigin in HeLa cells

(A) Schematic of GFP-tagged mVSP and RFP-tagged basigin constructs.

(B–F) Fluorescence images (left) and their corresponding intensity profiles (right) of the marked regions are shown for cells transfected singly with (B) GFP-tagged mVSP or (C) RFP-tagged basigin or (D) co-transfected with both or co-transfected with GFP-tagged mVSP and RFP-tagged PLCδ1-PH (a PM marker) in the (E) absence or (F) presence of exogenous Myc-tagged basigin (green, GFP; red, RFP).

(G) Surface expression analysis of VSP with and without exogenous basigin. Mean ± SEM, −basigin (control), $n = 19$ cells, three experiments; +basigin, $n = 18$ cells, three experiments; $^{****}p < 0.0001$; unpaired t test: $p = <0.0001$. Scale bars: 10 μm.

(H) Confocal microscopy.

(I) Antibody labeling of HeLa cells transfected with the GFP-mVSP-Ex HA construct in the absence (left) and presence of exogenous Myc-tagged basigin (right).

(J) Schematic of the extracellular HA tag and the intracellular GFP tag located on mVSP.

(K) Mock-transfected cells served as negative controls. Similar results were obtained in 3 transfections. Scale bars: 10 μm.

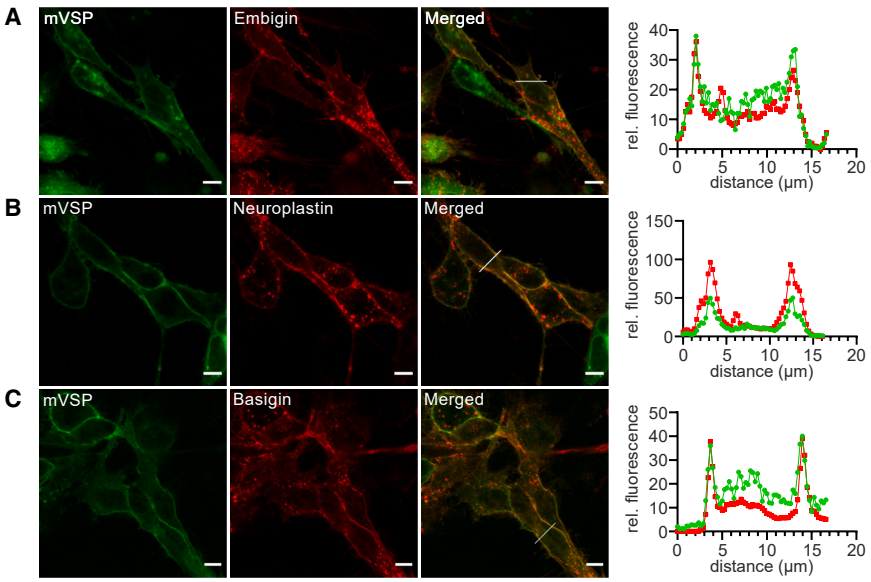

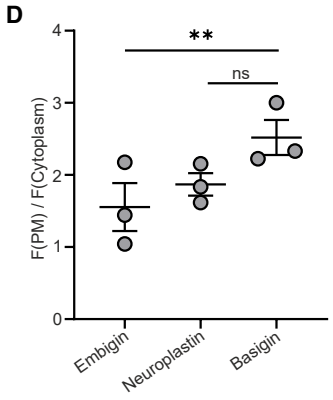

Figure 3. Co-localization of mVSP with basigin family members

(A–C) Live-cell imaging of HeLa cells co-transfected with GFP-tagged mVSP and RFP-tagged (A) embigin (EMB), (B) neuroplastin (NPTN), and (C) basigin (BSG) with their corresponding fluorescence intensity profiles (right) for a specified region, highlighted in the merged fluorescence images (left).

(D) Quantification of VSP surface expression in the presence of exogenous embigin, neuroplastin, or basigin. Mean ± SEM; basigin (control), $n = 20$ cells; neuroplastin, $n = 17$ cells; and embigin, $n = 18$ cells in three independent experiments each. $^{**}p < 0.01$; ns., not significant; Dunnett's test: neuroplastin, $p = 0.3053$; embigin, $p = 0.0067$. All images were taken 48 h post transfection. Scale bars: 10 μm.

the extra- and intracellular domains but must rely on the TM region of basigin. Sequence comparison shows that the TM domains of basigin, neuroplastin, and embigin are highly similar and include a conserved conspicuous glutamate residue (E222) in the center of the membrane-spanning region (Figure S7). We thus mutated the central glutamate and analyzed mVSP trafficking. Co-expression of the mutants with mVSP showed that while a conservative, charge-preserving mutation (E222D) did not change basigin's capability to mediate mVSP trafficking (Figures 5E and 5H), neutralization (E222Q) or charge reversal (E222K) largely abolished basigin-dependent forward trafficking of mVSP to the PM (Figures 5F–5I). Of note, targeting of basigin itself to the PM was not affected by either of these mutations (Figures S6F–S6H). Co-immunoprecipitation experiments showed that the interaction with mVSP was abolished in the E222Q and E222K (Figure 5I). Hence, the TM segment of basigin, including the central negative residue, constitutes the protein-protein interaction interface with mVSP.

Consequently, the transmembrane region of mVSP (i.e., the VSD), should constitute the complementary interaction site. To test this prediction, we exploited the fact that PM localization of the non-mammalian Ci-VSP is independent of interaction with basigin (Figures S8A and S8C) and that basigin does not physically bind to Ci-VSP, as shown by co-immunoprecipitation (coIP) experiments (Figure S8I). We thus generated VSP chimeras in which either the C-terminal PD or the intracellular N terminus of mVSP was replaced by the homologous domain of Ci-VSP, yielding m/ci-VSP or ci/mVSP, respectively (Figures S8D, S8E, and S9). m/ci-VSP was retained in the ER in a manner similar to wild-type mVSP (Figure S8D), whereas ci/m-VSP showed PM localization, although a major fraction of the protein was localized to an intracellular perinuclear compartment, likely the Golgi apparatus (Figure S8E). Co-expression of either chimera with basigin resulted in robust translocation to the PM (Figures S8F–S8H), resulting in a PM/cytoplasm ratio similar to that observed with mVSP/basigin co-expression (Figures 2 and 3). These findings indicate that neither the N- nor the C-terminal intracellular domains of mVSP are required for the functional interaction with basigin. CoIP assays confirmed physical binding of both chimeras to basigin, comparable to mVSP (Figure S8I). Taken together, these findings demonstrate that the transmembrane VSD, but not the intracellular domains of mVSP, mediates the binding to the TM domain of basigin.

To further explore the structural basis of this interaction, we employed structure prediction models of AlphaFold (AF).[41–43] Figure 6A shows structures of voltage-sensing domains of mVSP and Ci-VSP in complex with the transmembrane helix of mouse basigin predicted by AF-Multimer).[42] In all predicted structures, basigin consistently forms contacts with S4 of VSPs (Figures S10B and S10C). We also used AF3[43] to predict structures of the complexes with the Ig domain and PD included (Figure S10B). This approach yielded higher variability compared to AF-Multimer and suggested direct interactions of basigin with

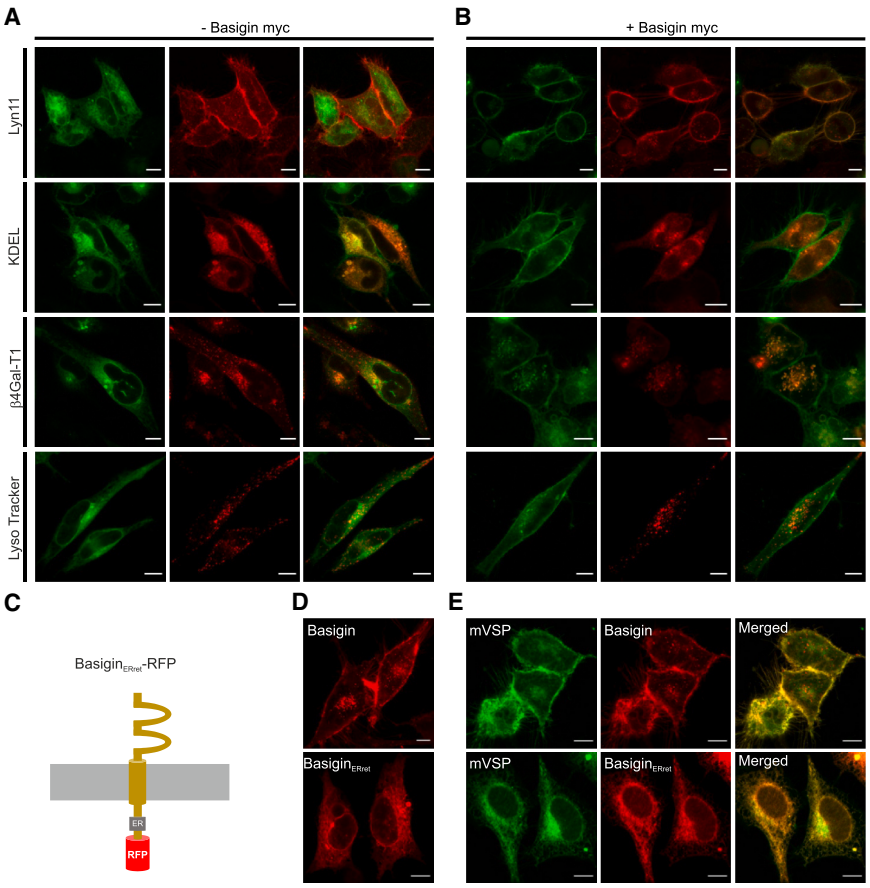

Figure 4. mVSP and basigin interaction and subcellular localization in HeLa Cells

(A and B) HeLa cells were co-transfected with GFP-tagged mVSP and RFP-tagged organelle markers (PM, PLCδ1-PH; ER, calreticulin; Golgi, beta-1,4-galactosyltransferase; lysosomes, LysoTracker) in the (A) absence and (B) presence of exogenous Myc-tagged basigin.

(C) Schematic of the ER retained basigin construct (basigin$_{ERret}$).

(D) Cells transfected with either RFP-tagged wild-type basigin (top) or its ER-retained mutant (bottom).

(E) Cells co-transfected with GFP-tagged mVSP and either wild-type RFP-tagged basigin or its ER-retained mutant.

All images were taken 48 h post transfection. Similar results were obtained in 3 transfections. Scale bars: 10 μm. Parts of the figure were created using Servier Medical Art, which is licensed under a Creative Commons Attribution 3.0 Unported License (https://creativecommons.org/licenses/by/3.0/).

S1 and S2 in addition to S4. Therefore, we focus on the interface formed by S4 of VSP consistently observed in both AF3- and AF-Multimer-predicted mVSP and Ci-VSP complexes.

In experimental cryoelectron microscopy (cryo-EM)-resolved structures of basigin and neuroplastin in complex with MCT1 (PDB: 6LZ0)[44] and PMCA1 (PDB: 6A69),[45] respectively, the TM helices mainly form contacts with a single TM helix of their interaction partner (Figure 6A). The overall arrangement in the basigin/mVSP complex is similar to these experimental structures. In contrast, the AF predictions for a basigin/Ci-VSP complex[45] indicate a rather poor alignment of basigin's TM with S4 with fewer interprotein contacts compared to mVSP (9 ± 2 vs. 17 ± 3) and misalignment of basigin with the principal axis of the VSD in Ci-VSP, which would infer an energetic penalty on the complex inserted into a membrane due to additional hydrophobic mismatch. Thus, the predictions are in line with the lack of basigin binding to Ci-VSP in the experimental data (Figures 6C–6E and S8I).

Interestingly, the conserved glutamate E222 is in close contact with the backbone of S4 in the predicted complexes with VSPs (Figure 6B), where it may form hydrogen bonds with the backbone oxygen atoms. This type of interaction is also observed in the experimental structure of neuroplastin with PMCA1, while in the basigin/MCT1 complex, the glutamate has a dedicated asparagine to form a hydrogen bond. We then analyzed the amino acid composition of the interaction interfaces. The alignment shown in Figure S10A indicates that the interfaces are mostly formed by hydrophobic residues and show no clear conservation among the studied interaction partners of basigin or neuroplastin. Highlighting the residues that are involved in the protein-protein interactions in every studied complex (Figure S10A) reveals that approximately every fourth residue of basigin/neuroplastin is in contact with an interaction partner. Thus, the interacting residues form a helical pattern so that basigin interacts with VSPs via a particular side of its transmembrane helix, which is conserved among the different basigin complexes.

Regulation of PM targeting by basigin evolved in the mammalian lineage

The archetypical non-vertebrate VSP, Ci-VSP, does not require the interaction with basigin for PM targeting (Figure 6C).[1,6,9] We therefore systematically assessed the interaction with basigin across the chordate phylogenetic tree by examining representative VSP orthologs from the vertebrate groups of fish, amphibians, and mammals.

As shown in Figure 6C, the representative VSP orthologs from sea squirt, zebrafish, and clawed frog all show robust PM localization in a mammalian expression system, in contrast to the intracellular retention of mammalian VSP. Co-expression of basigin did not change this subcellular localization, except for the mouse ortholog, as described above (Figure 6D). To analyze any association with basigin independent of a requirement for PM trafficking, we co-expressed each ortholog with basigin$_{ERret}$ (Figure 4C). As shown in Figure 6E, the PM localization of Ci-VSP, as well as of fish and amphibian VSPs, was unaffected by basigin$_{ERret}$, indicating that BSG association is a unique feature of mammalian

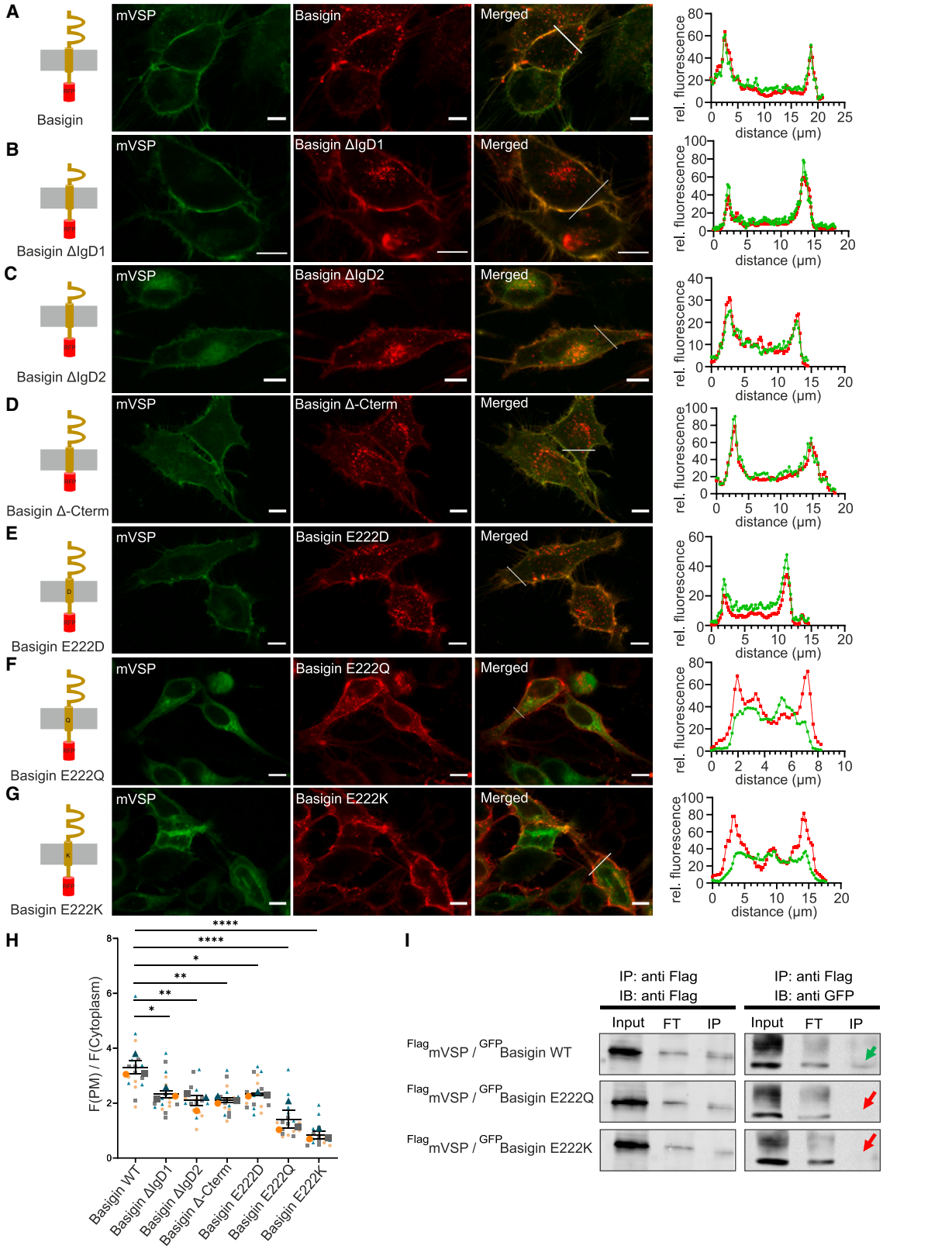

(legend on next page)

VSPs but not of other vertebrate VSPs. These findings outline an evolutionary trajectory in which the regulatory interaction with basigin emerged in the mammalian lineage.

Voltage-dependent phosphatase activity of mVSP unlocked by membrane targeting

PM targeting mediated by basigin provided the opportunity to explore the functional behavior of a native mammalian VSP. We examined the lipid phosphatase activity of mVSP in a live-cell assay by combining fluorescence biosensors for VSP's substrates measured by total internal reflection fluorescence (TIRF) microscopy[9] and control of the cell membrane potential by variation of the extracellular K^+ concentration (K^+_{ex}).[46] To facilitate the latter approach, we used a HEK293 cell line stably expressing the ROMK2 K^+ channel,[47] which confers large constitutive K^+ permeability, enabling setting membrane potentials close to the K^+ reversal potential (i.e., estimated −115 mV versus 0 mV at 2 mM and 150 mM K^+_{ex}, respectively). The $PI(4,5)P_2$ sensor PLCδ1-PH-GFP was used to address $PI(4,5)P_2$ phosphatase activity, as reported previously for non-mammalian VSPs.[6] First, to confirm the sensitivity of the assay, Ci-VSP was co-expressed with the sensor. Depolarization of the membrane potential by application of 150 mM K^+_{ex} resulted in a reversible decrease of PM-associated fluorescence, reporting dissociation of PLCδ1-PH-GFP from the membrane and therefore depletion of $PI(4,5)P_2$ (Figures 7A and 7D). When mVSP and basigin were co-expressed, depolarization induced robust translocation of the $PI(4,5)P_2$ sensor, indicating $PI(4,5)P_2$ depletion by mVSP (Figures 7A and 7B). No dissociation of PLCδ1-PH-GFP was observed when mutant mVSP (C458S) was expressed, which is catalytically inactivated by an amino acid exchange in the catalytic CX_5R motif[9,48,49] (Figures 7A and 7C). We observed equivalent results using a different $PI(4,5)P_2$ sensor, tubbyCT (Figure S11A). Thus, mVSP is a depolarization-activated $PI(4,5)P_2$ phosphatase *in vivo*.

We further probed for potential $PI(3,4,5)P_3$ phosphatase activity by monitoring buildup of the product of $PI(3,4,5)P_3$ dephosphorylation, $PI(3,4)P_2$, with the specific sensor TAPP1-PH-GFP.[50] When Ci-VSP was used as a positive control, TAPP1-PH-GFP strongly associated with the PM upon depolarization with 150 mM K^+ (Figures 7E and 7H). In cells co-expressing mVSP and basigin, depolarization also consistently increased membrane association of TAPP1-PH-GFP, indicating production of $PI(3,4)P_2$, revealing dephosphorylation of $PI(3,4,5)P_3$ at the 5 position (Figures 7E and 7F). This activity was completely absent when mVSP C458S was expressed (Figures 7E and 7G).

To obtain quantitative insights into the voltage sensitivity of mVSP, we next measured phosphatase activity through the TIRF microscopy assay across a range of membrane potentials (V_M) adjusted by varying K^+_{ex}. Figure 7I shows whole-cell patch-clamp recordings of V_M during application of various concentrations of K^+_{ex}, revealing that, in HEK cells expressing the constitutively open K^+ channel ROMK2, membrane potential closely follows the predicted equilibrium potential of K^+. Thus, this approach allowed for the precise and graded variation of V_M. As shown in Figures 7J and 7K, in ROMK-expressing cells transfected with mVSP/basigin or Ci-VSP together with the $PI(4,5)P_2$ sensor, larger increases in K^+_{ex} (i.e., stronger depolarization) resulted in the gradual increase of phosphatase activity. This growth function reveals the voltage sensitivity of each VSP ortholog. Of note, closer inspection of the changes in activity suggested that, even though maximal activity at 150 mM K^+_{ex} (approximately 0 mV) was somewhat smaller on average, the activity at moderate depolarization (15 and 50 mM K^+_{ex}) was stronger in mVSP/basigin-expressing cells compared to Ci-VSP (Figures 7J and 7K). Normalization to maximal activity (at 150 mM K^+_{ex}), shown in Figure 7L, reveals a clearly stronger activation at depolarization to approximately −50 and −25 mV, indicating a significantly more negative activation range of mVSP compared to Ci-VSP.

The observed difference from Ci-VSP could be an intrinsic property of the mammalian VSP or might alternatively be conferred by the association with basigin. We therefore sought to test a potential impact of basigin on the voltage sensitivity of mVSP. Since a direct approach was hampered by the lack of PM-localized mVSP in the absence of basigin, we made use of a minimally changed mVSP construct that is trafficked to the PM even in the absence of basigin. Replacement of the N terminus with that of Ci-VSP (chimera ci/mVSP) resulted in robust PM localization while structurally retaining the voltage sensor and PD of mVSP and functionally retaining the interaction with basigin (Figure S8). Activity measurements performed with the slightly more sensitive $PI(4,5)P_2$ probe tubbyCT-RFP (Figure S11) confirm the same negative activation voltage range for this mVSP construct, as shown in Figures 7M and 7N. Importantly, co-expression of basigin did not affect voltage sensitivity (Figure 7N).

In summary, mVSP is a voltage-activated PI 5-phosphatase recapitulating essential features known previously for non-mammalian VSPs but with a substantially left-shifted voltage activation. Moreover, basigin controls activity of mVSP by regulating its surface localization but not by modulating voltage sensitivity.

Figure 5. Mapping of the mVSP binding site on basigin

(A–G) Schematic (left) of RFP-tagged basigin mutants used in the experiments and the corresponding confocal images (center) of HeLa cells co-transfected with GFP-tagged mVSP and (A) basigin wild type (WT), (B) basigin ΔIgD1, (C) basigin ΔIgD2, (D) basigin ΔC-term, (E) basigin-E222D, (F) basigin- E222Q, and (G) basigin-E222K constructs and their corresponding fluorescence intensity profiles (right) for the specified region.

(H) Quantification of mVSP surface expression in the presence of exogenous basigin mutants. Mean ± SEM; basigin (control), $n = 15$ cells; basigin ΔIg, $n = 15$ cells; basigin ΔC-term, $n = 15$ cells; basigin E222D, $n = 15$ cells; basigin E222Q, $n = 15$ cells; and basigin E222K, $n = 15$ cells in three independent experiments each. ****$p < 0.0001$; *$p < 0.05$; Dunnett's test: basigin ΔIgD1 $p = 0.0124$; basigin ΔIgD2 $p = 0.0024$; basigin ΔC-term, $p = 0.0027$; basigin E222D, $p = 0.0119$; basigin E222Q, $p \leq 0.0001$; basigin E222K, $p \leq 0.0001$.

(I) CoIP was performed, similar to that shown in Figure 2, using the basigin mutants (E222Q and E222K). Observed bands were approximately 74 kDa for FLAG-tagged mVSP and approximately 65 kDa for GFP-tagged basigin and its mutants, consistent with their expected molecular weights. Images were acquired 48 h post transfection. Scale bars: 10 μm.

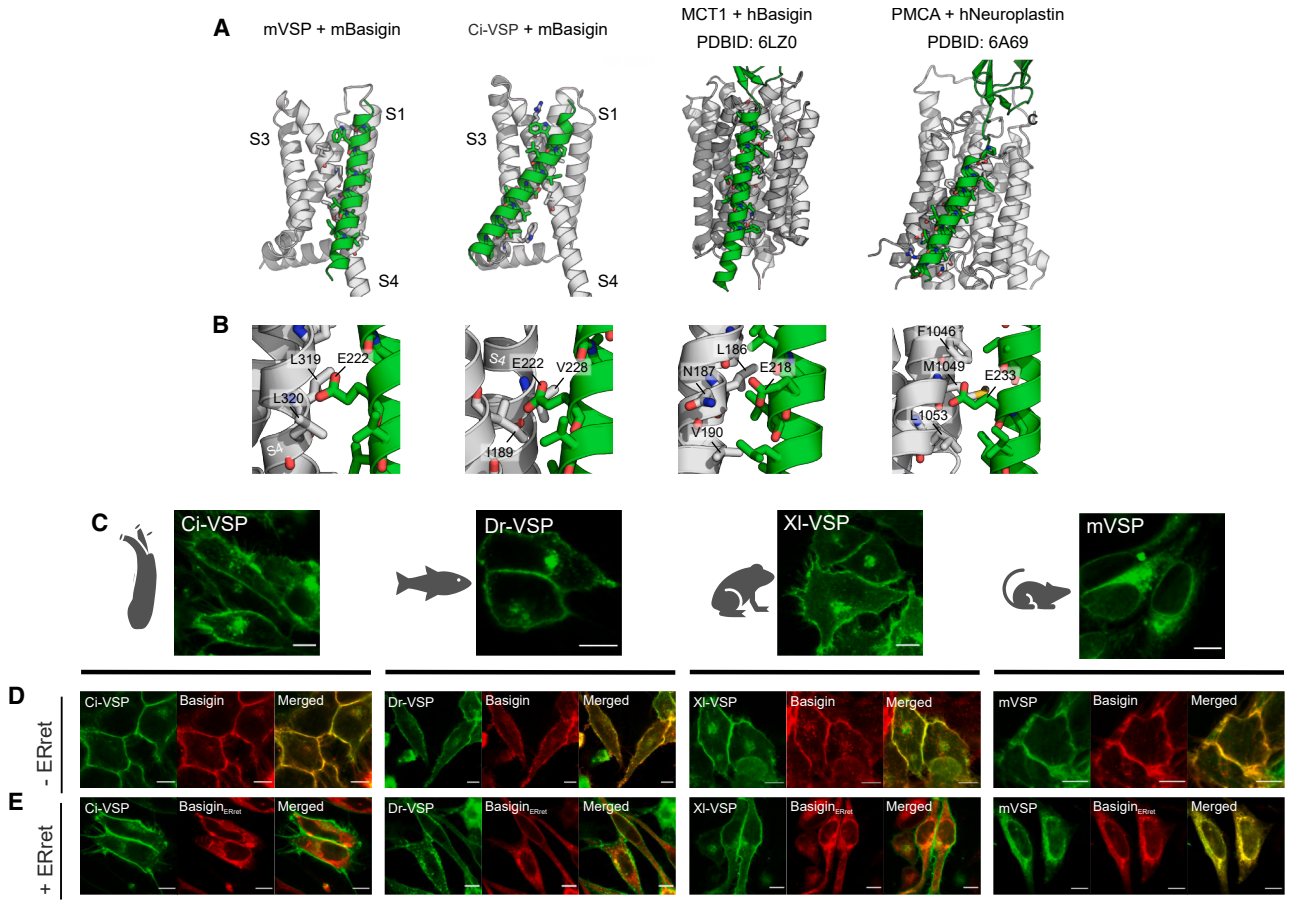

Figure 6. Comparative structural models and mammalian lineage-specific evolution of basigin's targeting function

(A) Structures of mVSP, Ci-VSP, MCT, and PMCA (white) in complex with basigin or neuroplastin (green). Residues that form the interaction interface are shown as sticks. Complexes of mVSP and Ci-VSP with mBasigin were predicted with AF-Multimer, with only transmembrane regions of the proteins used for the structure prediction.

(B) Closer view of the conserved glutamate residue as part of the interaction interface.

(C–E) HeLa cells were transfected with either (C) GFP-tagged Ci-VSP, *Danio rerio* (Dr)-VSP, *Xenopus laevis* (X)-VSP, or mVSP alone or (D) co-transfected with wild-type RFP-tagged basigin and (E) with an RFP tagged ER-retained basigin mutant. Images were acquired 48 h post transfection. Similar results were obtained in 3 transfections. Scale bars: 10 μm.

DISCUSSION

Non-mammalian VSPs have been studied extensively at the molecular level, revealing enzymatic specificity and deep insights into the mechanism of activation by membrane voltage. Making use of their potential to rapidly, reversibly, and gradually alter the cellular concentrations of PI levels in the PM, VSPs from *Ciona* and zebrafish have been widely adopted as highly useful tools to probe the cell biology of PIs.[12,46,50,51] These VSPs have also been engineered to improve the potency to manipulate cellular $PI(4,5)P_2$.[52]

Much less is known about mammalian VSPs. At least one VSP gene is present in all mammalian genomes, yet these proteins have remained largely uncharacterized because of lack of membrane localization in any heterologous expression system studied so far,[9,15,23,25,53] which has prevented the assessment of enzymatic properties and voltage dependence. Here, we resolve some of the open questions, using mouse VSP as the model for mammalian VSPs. Our key finding is that, by association with the single-TM proteins basigin, neuroplastin, or embigin, mVSP is trafficked to the PM rather than retained in the ER.

Mechanism of basigin-dependent forward trafficking

Intriguingly, basigin and its homologs have a similar effect on the PM trafficking of two unrelated groups of proteins, the PMCAs[39] and MCTs.[40,54,55] In either case, the underlying mechanism that enables PM localization remains unknown so far. However, for PMCA, assembly of a PMCA/neuroplastin complex in the ER and therefore co-trafficking to the PM has been shown by subcellular proteomic analysis of PMCA complexes.[39] Likewise, assembly of the basigin-MCT complex in the ER as a requirement for MCT trafficking to the PM has been proposed.[40]

Similarly, our findings indicate assembly of a VSP/basigin complex in the ER. Thus, basigin and neuroplastin constructs with ER-restricted localization did not facilitate forward trafficking of mVSP

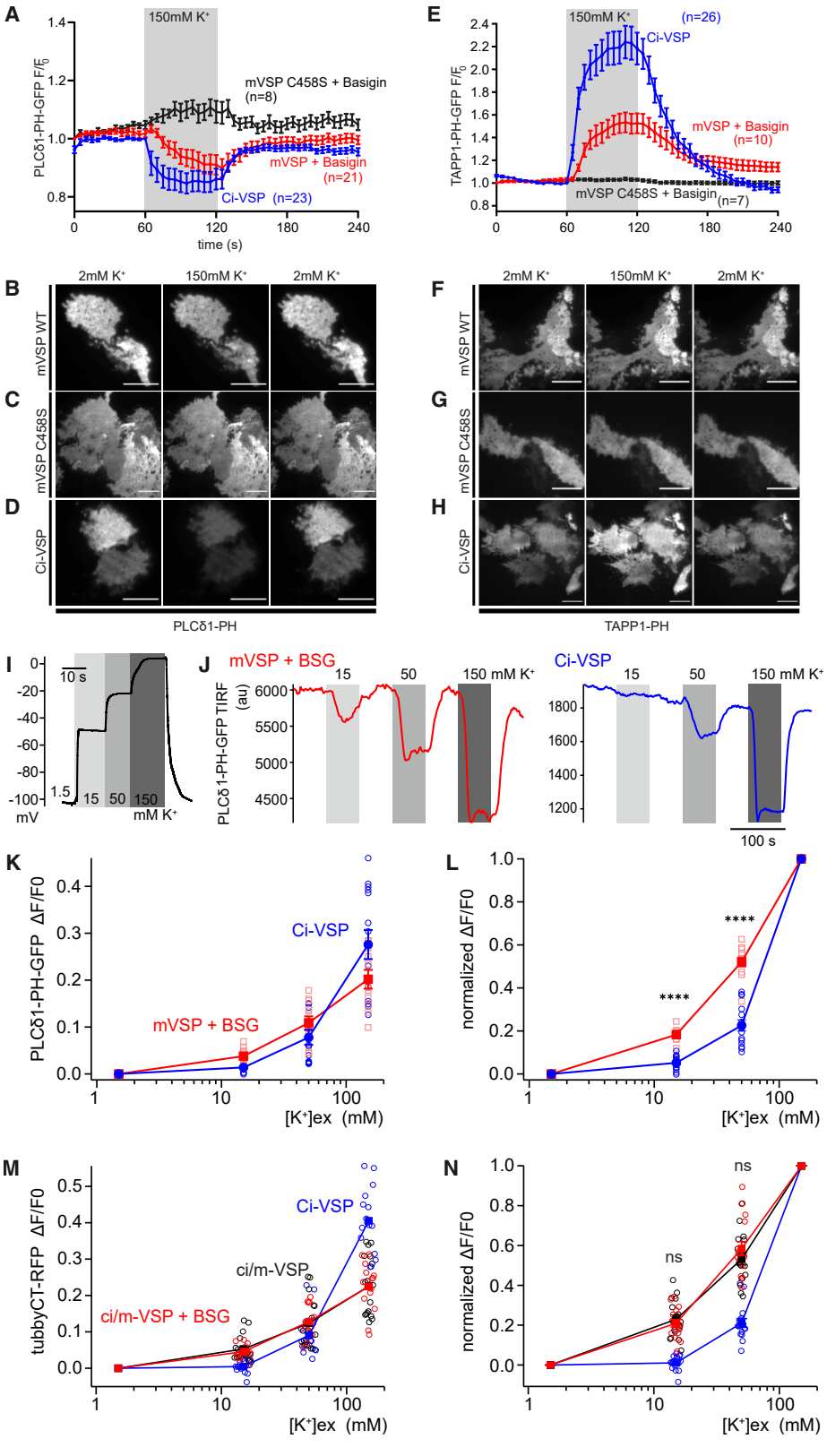

(legend on next page)

but closely colocalized with mVSP in the ER (Figures 4E and S5B). The extensive subcellular co-localization of both proteins and the stable physical association of both proteins shown by Y2H and coIP analysis indicate that both proteins traffic as a stable heteromeric complex through the secretory pathway from ER to PM.

The structural basis for the formation of heteromers of basigin family members and their cargo proteins is similar for all three cargo protein classes. Thus, binding of neuroplastin to PMCA[45] and basigin or embigin to MCTs[44,54] via TM-TM interaction has been directly observed in experimental structures obtained by cryo-EM. Our findings indicate an equivalent binding mechanism, as mutations in basigin's TM domain disrupted the functional and biochemical interaction, whereas the intra- and extracellular domains of basigin, including the Ig-like domains, were not required (Figure 5). Consistently, the interaction with basigin was independent of the intracellular domains of mVSP, indicating binding of basigin to the transmembrane VSD domain of mVSP (Figure S8).

Taken together, the similarity in the biochemical binding mode and the control of forward trafficking to the PM in three structurally unrelated classes of membrane proteins indicate a general principle of action. Thus, the basigin protein family (BSG, NPT, and EMB) appears to constitute a common trafficking hub for proteins destined for PM delivery. It will be interesting to see whether additional PM-localized membrane proteins rely on basigin or its homologs for trafficking. The mechanism of interaction with sorting and trafficking machinery is currently not known and certainly warrants further examination.

Catalytic function of mammalian VSP and voltage dependence

So far, evidence of the enzymatic activity of mammalian VSPs came from studies on chimeric proteins where the catalytic domain of human VSP1 was artificially fused to the VSD of non-mammalian VSPs[9,25] or, most recently, on a construct based on mVSP with modified VSD and exchange of the N terminus.[56] In these chimeras, the catalytic domain showed enzymatic activity as a PI phosphatase similar to non-mammalian VSPs, and activity was under control of the altered VSD.

Successful membrane trafficking mediated by basigin now enabled us to assess the catalytic function of a native mammalian VSP in the cellular environment. Our results show that mVSP is a PI 5-phosphatase that dephosphorylates both $PI(4,5)P_2$, as shown by depletion of $PI(4,5)P_2$ upon activation, and $PI(3,4,5)P_3$, as shown by production of $PI(3,4)P_2$ (Figure 7). Importantly, we also find that mVSP is controlled by membrane depolarization, being inactive at resting membrane potential and activated by depolarization (Figure 7). Taken together, mammalian VSP targeted to the PM exhibits the canonical features of well-studied non-mammalian VSPs.

Biological function of mammalian VSP and its interaction with basigin

A role of VSP in mouse sperm function was identified recently,[24,56] based on the observation that sperm from VSP knockout mice display impaired motility. Mechanistically, this phenotype has been attributed to a major role of VSP in shaping the sperm phospholipid profile. First, mature sperm from VSP knockout mice lack a polarized distribution of $PI(4,5)P_2$ that may be required to regulate ion channel activity and Ca^{2+} signaling.[24] Secondly, Kawai et al. found that developmental changes in $PI(4,5)P_2$ concentration during sperm maturation are affected by loss of VSP. Thus, in wild-type sperm, a high $PI(4,5)P_2$/PI(4)P ratio found in testicular sperm declined subsequently toward lower $PI(4,5)P_2$ levels in the epididymis. This developmental pattern was abolished in VSP knockout (KO) mice, suggesting that VSP phosphatase activity is the major determinant of low $PI(4,5)P_2$ in mature mouse sperm.[56] These observations suggested constitutive activity of VSP in maturing and mature sperm rather than acute/dynamic regulation by electrical signaling, and experimental approaches to alter membrane potential did not reveal dynamic changes in $PI(4,5)P_2$ levels.[56] V_M was determined to be strongly depolarized (around −10 mV), in epididymal sperm.[24,56,57] How does this compare to the activation behavior of mVSP? Whereas non-mammalian VSPs are only slightly activated at such depolarized V_M, here we describe the strong activation of mVSP even at substantially more negative V_M (estimated −50 to –25 mV). Thus mammalian VSP may be optimized for constitutive activation in maturing sperm, supporting tonic depletion of $PI(4,5)P_2$. It is worth noting, though, that the membrane potential of mammalian sperm hyperpolarizes upon capacitation (to around −65 mV).[3,58,59]

Figure 7. Phosphatase activity and voltage sensitivity of mVSP

(A) TIRF changes evoked by depolarization with 150 mM K^+_{ex} (gray shading) from ROMK2-Flp-In 293 cells expressing RFP-mVSP plus Myc-basigin (red), catalytically inactivated RFP-mVSP C458S plus Myc-basigin (black), or RFP-Ci-VSP (blue), together with the $PI(4,5)P_2$ sensor PLCδ1-PH-GFP. Traces show the mean time course of fluorescence normalized to initial fluorescence intensity (F/F_0) (±SEM).

(B–D) Representative PLCδ1-PH-GFP TIRF images from measurements as in (A) for each VSP construct before, during, and after application of 150 mM K^+_{ex}. Scale bar: 10 μm.

(E) Depolarization-induced changes of membrane association of the $PI(3,4)P_2$ sensor TAPP1-PH-GFP obtained with the same VSP constructs as in (A).

(F–H) Representative TAPP1-PH-GFP TIRF images for each VSP construct before, during, and after application of 150 mM K^+_{ex}.

(I) Recording of V_M from a non-transfected ROMK2-Flp-In 293 cell by whole-cell patch-clamping during application of the indicated different K^+_{ex} concentrations.

(J) Representative TIRF measurements (PLCδ1-PH-GFP) from ROMK2-Flp-In293 cells expressing RFP-mVSP plus basigin (left) or RFP-Ci-VSP (right) during application of K^+_{ex}, as indicated by shaded areas.

(K) $\Delta F/F_0$ responses from 11 cells (mVSP/basigin, red) and 14 cells as shown in (J), from 4 independent experiments each.

(L) TIRF responses from (K) were normalized to the F/F_0 response at 150 mM K^+_{ex} for each individual recording. ****$p < 0.0001$ for comparison of mVSP versus Ci-VSP (t test).

(M) VSP activity measurements recorded as in (K) from ROMK2-Flp-In293 cells expressing either an mVSP construct in which the N terminus was replaced with the N terminus of Ci-VSP (GFP-ci/mVSP, black; Figure S10; $n = 18$ cells), GFP-ci/mVSP plus Myc-basigin (red, $n = 16$), or GFP-Ci-VSP (blue, $n = 16$). tubbyCT-RFP was used as the $PI(4,5)P_2$ sensor. Recordings from 4 independent experiments for each condition.

(N) Data from (M) plotted normalized to F/F_0 response at 150 mM K^+_{ex}. ns indicates lack of significantly different responses from ci/mVSP in the presence versus absence of basigin (t test). Mean responses (±SEM) are shown as filled symbols, and individual recordings are plotted as open symbols.

Whether this affects $PI(4,5)P_2$ levels through deactivation of VSP remains to be addressed.

In the light of potential tonic activation of VSP, our current findings suggest an alternative or additional level of regulation of mammalian VSP through control of PM localization by basigin. Of note, expression and localization of mVSP largely recapitulate the spatial cellular distribution as well as the developmental importance of basigin in sperm and in spermatogenesis, respectively. Thus, early studies localized mVSP transcript and protein to spermatocytes and early spermatids.[23,53] It is well established that basigin is required for spermatogenesis during these phases and that KO of basigin results in lack of mature sperm (azoospermia).[60] However, this phenotype observed in basigin KO mice is more severe than that observed in the mVSP null mouse, indicating that basigin has other functions beyond trafficking of mVSP. Intriguingly, membrane transporters known to depend on basigin for trafficking are also required either for sperm development (MCT1/2, for lactate uptake during sperm development[61]) or function (PMCA[62,63]). On the other hand, VSP function may be less relevant for spermatogenesis, or compensatory mechanisms ensure proper development in the absence of VSP.

Notably, at the subcellular level, localization of mVSP to segments of the sperm tail corresponds to the subcellular distribution of basigin, as shown by sperm cell fractionation, even though the biochemical interaction of both proteins was unknown and not addressed.[24] Given our present results, we propose a likely functional role of basigin-mVSP interaction in developing and/or maturing sperm, specifically in facilitating the targeting of mVSP to the PM of the sperm tail. Future studies will be required to scrutinize the mVSP-BSG interaction in the native context and to resolve the complete interactome of VSP in sperm.

Finally, we emphasize that regulation of mVSP localization and, therefore, function by basigin was acquired only late in evolution, which may reflect specific functional requirements imposed by the unique mammalian reproductive physiology.

Limitations of the study

A major limitation of this study is that we lack a reliable antibody against mVSP, which restricts the ability to assess its endogenous localization and validate the interaction with basigin under native conditions. Although the predictions of mVSP-BSG complexes by AF are consistent with the experimental results, including absence of detectable binding to Ci-VSP, we note that the structure predictions do not take into account effects of unknown protein and lipid environments that may further affect complex formation. Specifically, dimerization through the VSD[64] may contribute to the low binding propensity of basigin to Ci-VSP.

Moreover, we note that the current data are focused on the mouse ortholog; thus, more comparative work will be needed to generalize the conclusions for mammalian VSPs.

RESOURCE AVAILABILITY

Lead contact

Requests for further information and resources should be directed to the lead contact, Dominik Oliver (oliverd@staff.uni-marburg.de).

Materials availability

All unique/stable reagents generated in this study are available from the lead contact without restriction.

Data and code availability

- Source data have been deposited at Figshare and are publicly available as of the date of publication at https://doi.org/10.6084/m9.figshare.29665130.
- This paper does not report original code.
- Any additional information required to reanalyze the data reported in this paper is available from the lead contact upon request.

ACKNOWLEDGMENTS

We thank Olga Ebers, Galina Zielke, and Nesli Oezen for excellent technical assistance. We gratefully acknowledge the gifts of mVSP from S.M. Bajjalieh, Ci-VSP and Dr-VSP from Y. Okamura, Xl-VSP from W. Ratzan, $NPTN_{ERret}$ from B. Fakler, PLCδ1-PH from T. Balla, Lyn11 from T. Meyer, tubby-Cterm from L. Shapiro, and TAPP1-PH from D. Alessi. This work was supported by grants from the von Behring-Röntgen-Stiftung (65-0028) to D.O., V.R., A.M., and S.B.; from the Deutsche Forschungsgemeinschaft (DFG; German Research Foundation) to V.R. (RE 4617/2-1), D.O. (OL 240/8-1 as part of the Research Unit FOR 5046, project P3), and J.-P.M. (MA 7525/2-2, as part of the Research Unit FOR 5046, project P2); and by the LOEWE Research Focus CoroPan (Project P5), funded by the State of Hesse, Germany (to V.R. and A.R.) The authors gratefully acknowledge the computing time granted through JARA on the supercomputer JURECA at Forschungszentrum Jülich under grant mpogt.

AUTHOR CONTRIBUTIONS

Conceptualization, V.R and D.O.; data curation, I.G.S., D.O., and V.R.; formal analysis, I.G.S., A.R., V.R., and D.O.; funding acquisition, D.O., V.R., A.M., S.B., and J.-P.M.; investigation, I.G.S., V.R., A.R., J.J., C.R.H., M.G., W.Z., and D.O.; computational structural analysis, A.Y.K.; methodology, V.R. and D.O.; resources, S.W.; supervision, V.R. and D.O.; visualization, I.G.S., V.R., and D.O.; writing – original draft, V.R. and D.O.; writing – review & editing, I.S., V.R., and D.O.

DECLARATION OF INTERESTS

The authors declare no competing interests.

STAR★METHODS

Detailed methods are provided in the online version of this paper and include the following:

- KEY RESOURCES TABLE
- EXPERIMENTAL MODEL AND STUDY PARTICIPANT DETAILS
  - Cell culture
- METHOD DETAILS
  - Molecular cloning and mutagenesis
  - Split-ubiquitin membrane yeast two-hybrid assay
  - Co-immunoprecipitation
  - Surface quantification assay in HeLa cells
  - Confocal microscopy
  - Quantitative assessment of mVSP localization in the PM through membrane-to-cytosol ratio calculation
  - Assessment of VSP activity by total internal reflection microscopy
  - Structure predictions
- QUANTIFICATION AND STATISTICAL ANALYSIS
  - Bioinformatics

SUPPLEMENTAL INFORMATION

Supplemental information can be found online at https://doi.org/10.1016/j.celrep.2025.116200.

Received: October 15, 2024
Revised: June 30, 2025
Accepted: August 5, 2025
Published: August 28, 2025

REFERENCES

1. Murata, Y., Iwasaki, H., Sasaki, M., Inaba, K., and Okamura, Y. (2005). Phosphoinositide phosphatase activity coupled to an intrinsic voltage sensor. Nature *435*, 1239–1243. https://doi.org/10.1038/nature03650.
2. Okamura, Y., Kawanabe, A., and Kawai, T. (2018). Voltage-Sensing Phosphatases: Biophysics, Physiology, and Molecular Engineering. Physiol. Rev. *98*, 2097–2131. https://doi.org/10.1152/physrev.00056.2017.
3. Arnoult, C., Kazam, I.G., Visconti, P.E., Kopf, G.S., Villaz, M., and Florman, H.M. (1999). Control of the low voltage-activated calcium channel of mouse sperm by egg ZP3 and by membrane hyperpolarization during capacitation. Proc. Natl. Acad. Sci. USA *96*, 6757–6762. https://doi.org/10.1073/pnas.96.12.6757.
4. Li, Q., Wanderling, S., Paduch, M., Medovoy, D., Singharoy, A., McGreevy, R., Villalba-Galea, C.A., Hulse, R.E., Roux, B., Schulten, K., et al. (2014). Structural mechanism of voltage-dependent gating in an isolated voltage-sensing domain. Nat. Struct. Mol. Biol. *21*, 244–252. https://doi.org/10.1038/nsmb.2768.
5. Villalba-Galea, C.A. (2012). Voltage-Controlled Enzymes: The New Janus-Bifrons. Front. Pharmacol. *3*, 161. https://doi.org/10.3389/fphar.2012.00161.
6. Halaszovich, C.R., Schreiber, D.N., and Oliver, D. (2009). Ci-VSP is a depolarization-activated phosphatidylinositol-4,5-bisphosphate and phosphatidylinositol-3,4,5-trisphosphate 5'-phosphatase. J. Biol. Chem. *284*, 2106–2113. https://doi.org/10.1074/jbc.M803543200.
7. Liu, L., Kohout, S.C., Xu, Q., Müller, S., Kimberlin, C.R., Isacoff, E.Y., and Minor, D.L., Jr. (2012). A glutamate switch controls voltage-sensitive phosphatase function. Nat. Struct. Mol. Biol. *19*, 633–641. https://doi.org/10.1038/nsmb.2289.
8. Matsuda, M., Takeshita, K., Kurokawa, T., Sakata, S., Suzuki, M., Yamashita, E., Okamura, Y., and Nakagawa, A. (2011). Crystal structure of the cytoplasmic phosphatase and tensin homolog (PTEN)-like region of Ciona intestinalis voltage-sensing phosphatase provides insight into substrate specificity and redox regulation of the phosphoinositide phosphatase activity. J. Biol. Chem. *286*, 23368–23377. https://doi.org/10.1074/jbc.M110.214361.
9. Halaszovich, C.R., Leitner, M.G., Mavrantoni, A., Le, A., Frezza, L., Feuer, A., Schreiber, D.N., Villalba-Galea, C.A., and Oliver, D. (2012). A human phospholipid phosphatase activated by a transmembrane control module. J. Lipid Res. *53*, 2266–2274. https://doi.org/10.1194/jlr.M026021.
10. Klein, R.M., Ufret-Vincenty, C.A., Hua, L., and Gordon, S.E. (2008). Determinants of molecular specificity in phosphoinositide regulation. Phosphatidylinositol (4,5)-bisphosphate (PI(4,5)P2) is the endogenous lipid regulating TRPV1. J. Biol. Chem. *283*, 26208–26216. https://doi.org/10.1074/jbc.M801912200.
11. Falkenburger, B.H., Jensen, J.B., and Hille, B. (2010). Kinetics of PIP2 metabolism and KCNQ2/3 channel regulation studied with a voltage-sensitive phosphatase in living cells. J. Gen. Physiol. *135*, 99–114. https://doi.org/10.1085/jgp.200910345.
12. Rjasanow, A., Leitner, M.G., Thallmair, V., Halaszovich, C.R., and Oliver, D. (2015). Ion channel regulation by phosphoinositides analyzed with VSPs-PI(4,5)P2 affinity, phosphoinositide selectivity, and PI(4,5)P2 pool accessibility. Front. Pharmacol. *6*, 127. https://doi.org/10.3389/fphar.2015.00127.
13. Keum, D., Kruse, M., Kim, D.I., Hille, B., and Suh, B.C. (2016). Phosphoinositide 5- and 3-phosphatase activities of a voltage-sensing phosphatase in living cells show identical voltage dependence. Proc. Natl. Acad. Sci. USA *113*, E3686–E3695. https://doi.org/10.1073/pnas.1606472113.
14. Iwasaki, H., Murata, Y., Kim, Y., Hossain, M.I., Worby, C.A., Dixon, J.E., McCormack, T., Sasaki, T., and Okamura, Y. (2008). A voltage-sensing phosphatase, Ci-VSP, which shares sequence identity with PTEN, dephosphorylates phosphatidylinositol 4,5-bisphosphate. Proc. Natl. Acad. Sci. USA *105*, 7970–7975. https://doi.org/10.1073/pnas.0803936105.
15. Walker, S.M., Downes, C.P., and Leslie, N.R. (2001). TPIP: a novel phosphoinositide 3-phosphatase. Biochem. J. *360*, 277–283. https://doi.org/10.1042/0264-6021:3600277.
16. Neuhaus, H., and Hollemann, T. (2009). Kidney specific expression of cTPTE during development of the chick embryo. Gene Expr. Patterns *9*, 568–571. https://doi.org/10.1016/j.gep.2009.09.002.
17. Ratzan, W.J., Evsikov, A.V., Okamura, Y., and Jaffe, L.A. (2011). Voltage sensitive phosphoinositide phosphatases of Xenopus: their tissue distribution and voltage dependence. J. Cell. Physiol. *226*, 2740–2746. https://doi.org/10.1002/jcp.22854.
18. Mutua, J., Jinno, Y., Sakata, S., Okochi, Y., Ueno, S., Tsutsui, H., Kawai, T., Iwao, Y., and Okamura, Y. (2014). Functional diversity of voltage-sensing phosphatases in two urodele amphibians. Physiol. Rep. *2*, e12061. https://doi.org/10.14814/phy2.12061.
19. Hossain, M.I., Iwasaki, H., Okochi, Y., Chahine, M., Higashijima, S., Nagayama, K., and Okamura, Y. (2008). Enzyme domain affects the movement of the voltage sensor in ascidian and zebrafish voltage-sensing phosphatases. J. Biol. Chem. *283*, 18248–18259. https://doi.org/10.1074/jbc.M706184200.
20. Chen, H., Rossier, C., Morris, M.A., Scott, H.S., Gos, A., Bairoch, A., and Antonarakis, S.E. (1999). A testis-specific gene, TPTE, encodes a putative transmembrane tyrosine phosphatase and maps to the pericentromeric region of human chromosomes 21 and 13, and to chromosomes 15, 22, and Y. Hum. Genet. *105*, 399–409. https://doi.org/10.1007/s004390051122.
21. Yamaguchi, S., Aoki, N., Kitajima, T., Okamura, Y., and Homma, K.J. (2014). Expression of the voltage-sensing phosphatase gene in the chick embryonic tissues and in the adult cerebellum. Commun. Integr. Biol. *7*, e9705021. https://doi.org/10.4161/19420889.2014.970502.
22. Ogasawara, M., Sasaki, M., Nakazawa, N., Nishino, A., and Okamura, Y. (2011). Gene expression profile of Ci-VSP in juveniles and adult blood cells of ascidian. Gene Expr. Patterns *11*, 233–238. https://doi.org/10.1016/j.gep.2010.12.004.
23. Tapparel, C., Reymond, A., Girardet, C., Guillou, L., Lyle, R., Lamon, C., Hutter, P., and Antonarakis, S.E. (2003). The TPTE gene family: cellular expression, subcellular localization and alternative splicing. Gene *323*, 189–199. https://doi.org/10.1016/j.gene.2003.09.038.
24. Kawai, T., Miyata, H., Nakanishi, H., Sakata, S., Morioka, S., Sasaki, J., Watanabe, M., Sakimura, K., Fujimoto, T., Sasaki, T., et al. (2019). Polarized PtdIns(4,5)P(2) distribution mediated by a voltage-sensing phosphatase (VSP) regulates sperm motility. Proc. Natl. Acad. Sci. USA *116*, 26020–26028. https://doi.org/10.1073/pnas.1916867116.
25. Rosasco, M.G., Gordon, S.E., and Bajjalieh, S.M. (2015). Characterization of the Functional Domains of a Mammalian Voltage-Sensitive Phosphatase. Biophys. J. *109*, 2480–2491. https://doi.org/10.1016/j.bpj.2015.11.004.
26. Rajan, S., Preisig-Müller, R., Wischmeyer, E., Nehring, R., Hanley, P.J., Renigunta, V., Musset, B., Schlichthörl, G., Derst, C., Karschin, A., and Daut, J. (2002). Interaction with 14-3-3 proteins promotes functional expression of the potassium channels TASK-1 and TASK-3. J. Physiol. *545*, 13–26. https://doi.org/10.1113/jphysiol.2002.027052.
27. Ficker, E., Dennis, A.T., Wang, L., and Brown, A.M. (2003). Role of the cytosolic chaperones Hsp70 and Hsp90 in maturation of the cardiac potassium channel HERG. Circ. Res. *92*, e87–e100. https://doi.org/10.1161/01.RES.0000079028.31393.15.
28. Manganas, L.N., and Trimmer, J.S. (2004). Calnexin regulates mammalian Kv1 channel trafficking. Biochem. Biophys. Res. Commun. *322*, 577–584. https://doi.org/10.1016/j.bbrc.2004.06.182.

29. Gee, H.Y., Tang, B.L., Kim, K.H., and Lee, M.G. (2010). Syntaxin 16 binds to cystic fibrosis transmembrane conductance regulator and regulates its membrane trafficking in epithelial cells. J. Biol. Chem. *285*, 35519–35527. https://doi.org/10.1074/jbc.M110.162438.

30. Abbott, G.W. (2022). Kv Channel Ancillary Subunits: Where Do We Go from Here? Physiology *37*, 225–241. https://doi.org/10.1152/physiol.00005.2022.

31. Capera, J., Serrano-Novillo, C., Navarro-Perez, M., Cassinelli, S., and Felipe, A. (2019). The Potassium Channel Odyssey: Mechanisms of Traffic and Membrane Arrangement. Int. J. Mol. Sci. *20*, 734. https://doi.org/10.3390/ijms20030734.

32. Toyama, Y., Maekawa, M., Kadomatsu, K., Miyauchi, T., Muramatsu, T., and Yuasa, S. (1999). Histological characterization of defective spermatogenesis in mice lacking the basigin gene. Anat. Histol. Embryol. *28*, 205–213. https://doi.org/10.1046/j.1439-0264.1999.00194.x.

33. Chen, H., Lam Fok, K., Jiang, X., and Chan, H.C. (2012). New insights into germ cell migration and survival/apoptosis in spermatogenesis: Lessons from CD147. Spermatogenesis *2*, 264–272. https://doi.org/10.4161/spmg.22014.

34. Muramatsu, T. (2016). Basigin (CD147), a multifunctional transmembrane glycoprotein with various binding partners. J. Biochem. *159*, 481–490. https://doi.org/10.1093/jb/mvv127.

35. Beesley, P.W., Herrera-Molina, R., Smalla, K.H., and Seidenbecher, C. (2014). The Neuroplastin adhesion molecules: key regulators of neuronal plasticity and synaptic function. J. Neurochem. *131*, 268–283. https://doi.org/10.1111/jnc.12816.

36. Ozawa, M., Huang, R.P., Furukawa, T., and Muramatsu, T. (1988). A teratocarcinoma glycoprotein carrying a developmentally regulated carbohydrate marker is a member of the immunoglobulin gene superfamily. J. Biol. Chem. *263*, 3059–3062.

37. MacGurn, J.A. (2014). Garbage on, garbage off: new insights into plasma membrane protein quality control. Curr. Opin. Cell Biol. *29*, 92–98. https://doi.org/10.1016/j.ceb.2014.05.001.

38. Jackson, M.P., and Hewitt, E.W. (2016). Cellular proteostasis: degradation of misfolded proteins by lysosomes. Essays Biochem. *60*, 173–180. https://doi.org/10.1042/EBC20160005.

39. Schmidt, N., Kollewe, A., Constantin, C.E., Henrich, S., Ritzau-Jost, A., Bildl, W., Saalbach, A., Hallermann, S., Kulik, A., Fakler, B., and Schulte, U. (2017). Neuroplastin and Basigin Are Essential Auxiliary Subunits of Plasma Membrane Ca(2+)-ATPases and Key Regulators of Ca(2+) Clearance. Neuron *96*, 827–838.e9. https://doi.org/10.1016/j.neuron.2017.09.038.

40. Kirk, P., Wilson, M.C., Heddle, C., Brown, M.H., Barclay, A.N., and Halestrap, A.P. (2000). CD147 is tightly associated with lactate transporters MCT1 and MCT4 and facilitates their cell surface expression. EMBO J. *19*, 3896–3904. https://doi.org/10.1093/emboj/19.15.3896.

41. Jumper, J., Evans, R., Pritzel, A., Green, T., Figurnov, M., Ronneberger, O., Tunyasuvunakool, K., Bates, R., Žídek, A., Potapenko, A., et al. (2021). Highly accurate protein structure prediction with AlphaFold. Nature *596*, 583–589. https://doi.org/10.1038/s41586-021-03819-2.

42. Evans, R., O'Neill, M., Pritzel, A., Antropova, N., Senior, A., Green, T., Žídek, A., Bates, R., Blackwell, S., Yim, J., et al. (2022). Protein complex prediction with AlphaFold-Multimer. Preprint at bioRxiv. https://doi.org/10.1101/2021.10.04.463034.

43. Abramson, J., Adler, J., Dunger, J., Evans, R., Green, T., Pritzel, A., Ronneberger, O., Willmore, L., Ballard, A.J., Bambrick, J., et al. (2024). Accurate structure prediction of biomolecular interactions with AlphaFold 3. Nature *630*, 493–500. https://doi.org/10.1038/s41586-024-07487-w.

44. Wang, N., Jiang, X., Zhang, S., Zhu, A., Yuan, Y., Xu, H., Lei, J., and Yan, C. (2021). Structural basis of human monocarboxylate transporter 1 inhibition by anti-cancer drug candidates. Cell *184*, 370–383.e13. https://doi.org/10.1016/j.cell.2020.11.043.

45. Gong, D., Chi, X., Ren, K., Huang, G., Zhou, G., Yan, N., Lei, J., and Zhou, Q. (2018). Structure of the human plasma membrane Ca(2+)-ATPase 1 in complex with its obligatory subunit neuroplastin. Nat. Commun. *9*, 3623. https://doi.org/10.1038/s41467-018-06075-7.

46. Mavrantoni, A., Thallmair, V., Leitner, M.G., Schreiber, D.N., Oliver, D., and Halaszovich, C.R. (2015). A method to control phosphoinositides and to analyze PTEN function in living cells using voltage sensitive phosphatases. Front. Pharmacol. *6*, 68. https://doi.org/10.3389/fphar.2015.00068.

47. Renigunta, A., Renigunta, V., Saritas, T., Decher, N., Mutig, K., and Waldegger, S. (2011). Tamm-Horsfall glycoprotein interacts with renal outer medullary potassium channel ROMK2 and regulates its function. J. Biol. Chem. *286*, 2224–2235. https://doi.org/10.1074/jbc.M110.149880.

48. Lacroix, J.J., and Bezanilla, F. (2012). Tuning the voltage-sensor motion with a single residue. Biophys. J. *103*, L23–L25. https://doi.org/10.1016/j.bpj.2012.06.030.

49. Maehama, T., Taylor, G.S., and Dixon, J.E. (2001). PTEN and myotubularin: novel phosphoinositide phosphatases. Annu. Rev. Biochem. *70*, 247–279. https://doi.org/10.1146/annurev.biochem.70.1.247.

50. Goulden, B.D., Pacheco, J., Dull, A., Zewe, J.P., Deiters, A., and Hammond, G.R.V. (2019). A high-avidity biosensor reveals plasma membrane PI(3,4)P(2) is predominantly a class I PI3K signaling product. J. Cell Biol. *218*, 1066–1079. https://doi.org/10.1083/jcb.201809026.

51. Lindner, M., Leitner, M.G., Halaszovich, C.R., Hammond, G.R.V., and Oliver, D. (2011). Probing the regulation of TASK potassium channels by PI4,5P(2) with switchable phosphoinositide phosphatases. J. Physiol. *589*, 3149–3162. https://doi.org/10.1113/jphysiol.2011.208983.

52. Kawanabe, A., Mizutani, N., Polat, O.K., Yonezawa, T., Kawai, T., Mori, M.X., and Okamura, Y. (2020). Engineering an enhanced voltage-sensing phosphatase. J. Gen. Physiol. *152*, e201912491. https://doi.org/10.1085/jgp.201912491.

53. Wu, Y., Dowbenko, D., Pisabarro, M.T., Dillard-Telm, L., Koeppen, H., and Lasky, L.A. (2001). PTEN 2, a Golgi-associated testis-specific homologue of the PTEN tumor suppressor lipid phosphatase. J. Biol. Chem. *276*, 21745–21753. https://doi.org/10.1074/jbc.M101480200.

54. Xu, B., Zhang, M., Zhang, B., Chi, W., Ma, X., Zhang, W., Dong, M., Sheng, L., Zhang, Y., Jiao, W., et al. (2022). Embigin facilitates monocarboxylate transporter 1 localization to the plasma membrane and transition to a decoupling state. Cell Rep. *40*, 111343. https://doi.org/10.1016/j.celrep.2022.111343.

55. Manoharan, C., Wilson, M.C., Sessions, R.B., and Halestrap, A.P. (2006). The role of charged residues in the transmembrane helices of monocarboxylate transporter 1 and its ancillary protein basigin in determining plasma membrane expression and catalytic activity. Mol. Membr. Biol. *23*, 486–498. https://doi.org/10.1080/09687860600841967.

56. Kawai, T., Morioka, S., Miyata, H., Andriani, R.T., Akter, S., Toma, G., Nakagawa, T., Oyama, Y., Iida-Norita, R., Sasaki, J., et al. (2024). The significance of electrical signals in maturing spermatozoa for phosphoinositide regulation through voltage-sensing phosphatase. Nat. Commun. *15*, 7289. https://doi.org/10.1038/s41467-024-51755-2.

57. Zeng, X.H., Yang, C., Kim, S.T., Lingle, C.J., and Xia, X.M. (2011). Deletion of the Slo3 gene abolishes alkalization-activated K+ current in mouse spermatozoa. Proc. Natl. Acad. Sci. USA *108*, 5879–5884. https://doi.org/10.1073/pnas.1100240108.

58. Wang, H., McGoldrick, L.L., and Chung, J.J. (2021). Sperm ion channels and transporters in male fertility and infertility. Nat. Rev. Urol. *18*, 46–66. https://doi.org/10.1038/s41585-020-00390-9.

59. Navarro, B., Kirichok, Y., and Clapham, D.E. (2007). KSper, a pH-sensitive K+ current that controls sperm membrane potential. Proc. Natl. Acad. Sci. USA *104*, 7688–7692. https://doi.org/10.1073/pnas.0702018104.

60. Bi, J., Li, Y., Sun, F., Saalbach, A., Klein, C., Miller, D.J., Hess, R., and Nowak, R.A. (2013). Basigin null mutant male mice are sterile and exhibit impaired interactions between germ cells and Sertoli cells. Dev. Biol. *380*, 145–156. https://doi.org/10.1016/j.ydbio.2013.05.023.

61. Bernardino, R.L., D'Souza, W.N., Rato, L., Rothstein, J.L., Dias, T.R., Chui, D., Wannberg, S., Alves, M.G., and Oliveira, P.F. (2019). Knockout of MCT1 results in total absence of spermatozoa, sex hormones dysregulation, and morphological alterations in the testicular tissue. Cell Tissue Res. *378*, 333–339. https://doi.org/10.1007/s00441-019-03028-4.

62. Schuh, K., Cartwright, E.J., Jankevics, E., Bundschu, K., Liebermann, J., Williams, J.C., Armesilla, A.L., Emerson, M., Oceandy, D., Knobeloch, K. P., and Neyses, L. (2004). Plasma membrane Ca2+ ATPase 4 is required for sperm motility and male fertility. J. Biol. Chem. *279*, 28220–28226. https://doi.org/10.1074/jbc.M312599200.

63. Okunade, G.W., Miller, M.L., Pyne, G.J., Sutliff, R.L., O'Connor, K.T., Neumann, J.C., Andringa, A., Miller, D.A., Prasad, V., Doetschman, T., et al. (2004). Targeted ablation of plasma membrane Ca2+-ATPase (PMCA) 1 and 4 indicates a major housekeeping function for PMCA1 and a critical role in hyperactivated sperm motility and male fertility for PMCA4. J. Biol. Chem. *279*, 33742–33750. https://doi.org/10.1074/jbc.M404628200.

64. Rayaprolu, V., Royal, P., Stengel, K., Sandoz, G., and Kohout, S.C. (2018). Dimerization of the voltage-sensing phosphatase controls its voltage-sensing and catalytic activity. J. Gen. Physiol. *150*, 683–696. https://doi.org/10.1085/jgp.201812064.

65. Ho, S.N., Hunt, H.D., Horton, R.M., Pullen, J.K., and Pease, L.R. (1989). Site-directed mutagenesis by overlap extension using the polymerase chain reaction. Gene *77*, 51–59. https://doi.org/10.1016/0378-1119(89)90358-2.

66. Iyer, K., Bürkle, L., Auerbach, D., Thaminy, S., Dinkel, M., Engels, K., and Stagljar, I. (2005). Utilizing the split-ubiquitin membrane yeast two-hybrid system to identify protein-protein interactions of integral membrane proteins. Sci. STKE *2005*, pl3. https://doi.org/10.1126/stke.2752005pl3.

67. Thaminy, S., Miller, J., and Stagljar, I. (2004). The split-ubiquitin membrane-based yeast two-hybrid system. Methods Mol. Biol. *261*, 297–312. https://doi.org/10.1385/1-59259-762-9:297.

68. Stagljar, I., Korostensky, C., Johnsson, N., and te Heesen, S. (1998). A genetic system based on split-ubiquitin for the analysis of interactions between membrane proteins in vivo. Proc. Natl. Acad. Sci. USA *95*, 5187–5192. https://doi.org/10.1073/pnas.95.9.5187.

69. Renigunta, V., Yuan, H., Zuzarte, M., Rinné, S., Koch, A., Wischmeyer, E., Schlichthörl, G., Gao, Y., Karschin, A., Jacob, R., et al. (2006). The retention factor p11 confers an endoplasmic reticulum-localization signal to the potassium channel TASK-1. Traffic *7*, 168–181. https://doi.org/10.1111/j.1600-0854.2005.00375.x.

70. Thallmair, V., Schultz, L., Zhao, W., Marrink, S.J., Oliver, D., and Thallmair, S. (2022). Two cooperative binding sites sensitize PI(4,5)P(2) recognition by the tubby domain. Sci. Adv. *8*, eabp9471. https://doi.org/10.1126/sciadv.abp9471.

STAR★METHODS

KEY RESOURCES TABLE

REAGENT or RESOURCE	SOURCE	IDENTIFIER
Antibodies		
GFP Antibody (B-2)	Santa Cruz Biotechnology	Cat#sc-9996; RRID: AB_627695
ANTI-FLAG® M2 antibody	Sigma-Aldrich	Cat#F1804; RRID: AB_262044
Myc-Tag (71D10) Rabbit mAb	Cell Signaling Technology	Cat#91856; RRID: AB_3073821
Anti-Human HA Monoclonal Antibody	Sigma-Aldrich	Cat#H3663; RRID: AB_262051
Lex A (2-12)	Santa Cruz Biotechnology	Cat# sc-7544; RRID AB_627883
IRDye 800CW Goat anti-Mouse IgG	LI-COR Biosciences	Cat#925-32210; RRID: AB_2687825
IRDye 800CW Goat anti-Rabbit IgG	LI-COR Biosciences	Cat#926-32211; RRID: AB_621843
RDye 800CW Goat anti-Rat IgG	LI-COR Biosciences	Cat#926-32219, RRID: AB_1850025
Goat anti-Mouse IgG (H+L) Highly Cross-Adsorbed Secondary Antibody, Alexa Fluor™ 488	Thermo Fisher Scientific	Cat#A-11029; RRID: AB_2534088
Goat anti-Mouse IgG (H+L) Highly Cross-Adsorbed Secondary Antibody, Alexa Fluor™ 594	Thermo Fisher Scientific	Cat#A-11032; RRID: AB_2534091
Mouse EMMPRIN/CD147 Antibody	R and D Systems	Cat#AF772; RRID: AB_355588
Donkey anti-goat IgG-HRP	Santa Cruz Biotechnology	Cat# sc-2020; RRID: AB_631728
Bacterial and virus strains		
Subcloning Efficiency™ DH5α Competent Cells	Thermo Fisher Scientific	Cat#18265017
Chemicals, peptides, and recombinant proteins		
Hygromycin B	Thermo Fisher Scientific	Cat#10687010
GelRed® Nucleic Acid Stain	Merck	Cat#SCT123
Protease-Inhibitor-Mix G	SERVA	Cat#39101
Triton® X 100	ROTH	Cat#3051.3
Poly(ethyleneglycol)	Sigma-Aldrich	Cat#81242
Minimal SD Base	Takara	Cat#630411
DO Supplement –Leu/–Trp	Takara	Cat#630417
DO Supplement –His/–Leu/–Trp	Takara	Cat#630419
DO Supplement –Ade/–His/–Leu/–Trp	Takara	Cat#630428
YPD Broth	ROTH	Cat#X970
Lithium acetate dihydrate	Sigma-Aldrich	Cat#L4158
Deoxyribonucleic acid from herring sperm	Sigma-Aldrich	Cat#D3159
jetPEI®	Polyplus	Cat#101000053
jetPRIME®	Polyplus	Cat#101000046
Critical commercial assays		
Anti-FLAG® M2 Magnetic Beads	Sigma-Aldrich	Cat#M8823
Y2H Membrane Protein Kit	MoBiTec GmbH	Cat#P01001DS
PfuUltra II Hotstart PCR Master Mix	Agilent	Cat#600852
Phusion High-Fidelity PCR Master Mix with HF Buffer	Thermo Scientific™	Cat#F531L
SuperSignal™ ELISA Femto Substrate	Thermo Scientific™	Cat#37075
Deposited data		
Source data	https://doi.org/10.6084/m9.figshare.29665130	N/A

(*Continued on next page*)

Continued

REAGENT or RESOURCE	SOURCE	IDENTIFIER
Experimental models: Cell lines		
HEK-293, Human	Cytion	Cat#CLS-300192
HeLa, Human	Biozol	Cat#ADD-C0008001
CHO-K1, hamster	Leibniz Institute DSMZ-German Collection of Microorganisms and Cell Cultures	Cat#ACC110
ROMK2-Flp-In 293 Cells	Renigunta et al.[47]	N/A
Experimental models: Organisms/strains		
Strain NMY51: [MATa his3Δ200 trp1-901 leu2-3,112 ade2 LYS2::(lexAop)4-HIS3 ura3::(lexAop)8-lacZ ade2::(lexAop)8-ADE2 GAL4]	MoBiTec GmbH	N/A
Oligonucleotides		
mVSP pBT3C for: 5'-aat agg cca tta cgg cca tgt atg gag aa-3'	This paper	N/A
mVSP pBT3C rev: 5'-att tgg ccg agg cgg ccc tgt tct cac caa a-3'	This paper	N/A
mBasigin-pPR3C-for: 5'-att ggc cat tac ggc ccg atg gcg gcg gcg ctg ctg-3'	This paper	N/A
mBasigin-pPR3C-rev: 5'-aat ggc cga ggc ggc cga ggt ggc gtt cct ctg-3'	This paper	N/A
mVSP-PEGFPC-for: 5'-gat ctc gag cta tgt atg gag aaa aga ag-3'	This paper	N/A
mVSP-PEGFPC-rev: 5'-ggt gga tcc tca ctg cag cta gtt ctc acc aaa-3'	This paper	N/A
mBasigin pRFPN for: 5'-gat ctc gag atg gcg gcg gcg ctg ctg-3'	This paper	N/A
mBasigin pRFPN rev: 5'-ggt gga tcc cgg gtg gcg ttc ct-3'	This paper	N/A
mVSP exHA for: 5'-gca ctt tat gac aaa cca ggc ggg tac cca tac gac gtc cca gat tac gct ggc ggg cct cac ttt ctc aga g-3'	This paper	N/A
mVSP exHA rev: 5'-ctc tga gaa agt gag gcc cgc cag cgt aat ctg gga cgt cgt atg ggt acc cgc ctg gtt tgt cat aaa gtg c-3'	This paper	N/A
Recombinant DNA		
mVSP-pEGFPC	This paper	Genbank: NM_199257.2
mVSP-pRFP	This paper	Genbank: NM_199257.2
mVSP-pBT3N	This paper	Genbank: NM_199257.2
mVSP-3xflag-pCDNA3.1	This paper	Genbank: NM_199257.2
mVSP-Ex-HA-pEGFP	This paper	Genbank: NM_199257.2
m/ci-VSP-pEGFP	This paper	N/A
ci/m-VSP-pEGFP	This paper	N/A
mBSG-pPR3C	This paper	Genbank: NM_001077184.1
mBSG-pRFP	This paper	Genbank: NM_001077184.1
mBSG-myc-pCDNA3.1	This paper	Genbank: NM_001077184.1
mBSG-3xflag-pCDNA3.1	This paper	Genbank: NM_001077184.1
mBSG-ERret-pRFP	This paper	N/A
mEMB-pRFP	This paper	Genbank: NM_010330.4
mEMB -ERret-pRFP	This paper	N/A
mNPTN-pRFP	This paper	Genbank: NM_009145.2

(*Continued on next page*)

Continued

REAGENT or RESOURCE	SOURCE	IDENTIFIER
mNPTN -ERret-pRFP	Schmidt et al.[39]	N/A
Ci-VSP-pEGFP	This paper	Genbank: AB183035.1
Ci-VSP-pRFP	Halaszovich et al.[6]	Genbank: AB183035.1
Dr-VSP-pEGFP	This paper	Genbank: AB308476.1
Xl-VSP-GFP-pCDNA3.1	Ratzan et al.[17]	N/A
PLCδ1-PH-pEGFP	Halaszovich et al.[6]	N/A
PLCδ1-PH-pRFP	This paper	N/A
TAPP1-PH-pEGFP	Halaszovich et al.[6]	N/A
TubbyCT-pEGFP	Halaszovich et al.[6]	N/A
pDsRed-Monomer-Golgi	Clontech	Cat#632480
pDsRed2-ER	Clontech	Cat#632409
Lyn11-RFP	This paper	N/A
pAI-Alg5	MoBiTec	N/A
pDL2-ALg5	MoBiTec	N/A
Software and algorithms		
Graphpad Prism 8.0	https://www.graphpad.com	N/A
Igor Pro	https://www.wavemetrics.com/	N/A
blastn	https://blast.ncbi.nlm.nih.gov/Blast.cgi	N/A
Clustal Omega	https://www.ebi.ac.uk/jdispatcher/msa/clustalo	N/A
SnapGene	https://www.snapgene.com/	N/A
Fiji	https://fiji.sc/	N/A
CorelDRAW Graphics Suite 2019	https://www.coreldraw.com/de/	N/A
LAS X	https://www.leica-microsystems.com/products/microscope-software	N/A
PatchMaster	https://www.heka.com/	N/A
Image Lab Software	https://www.bio-rad.com	N/A
Other		
AlphaFold	https://alphafoldserver.com	N/A
Servier Medical Art	https://smart.servier.com/	N/A

EXPERIMENTAL MODEL AND STUDY PARTICIPANT DETAILS

Cell culture

HeLa and HEK cells were cultured in high-glucose DMEM supplemented with 10% fetal calf serum (FCS; Life Technologies, Paisley, United Kingdom) and 1% penicillin/streptomycin (PAA Laboratories, Pasching, Austria), and were transiently transfected using jetPRIME reagent (Polyplus), according to the manufacturer's instructions. For live-cell imaging using confocal microscopy, cells were seeded into 35 mm dishes (Greiner Bio-one GmbH, Frickenhausen, Germany) containing coverslips. CHO cells were maintained in MEM Alpha Medium supplemented with 10% FCS and 1% penicillin/streptomycin (Invitrogen GmbH, Darmstadt, Germany) and transfected with jetPEI transfection reagent (Polyplus Transfection, Illkirch, France). ROMK2 Flp-In 293 cells stably expressing ROMK2 were cultured in high-glucose DMEM with 10% FCS, 1% penicillin/streptomycin, and hygromycin for selection. For TIRF microscopy and high K^+ depolarization experiments, these cells were seeded into μ-Slide VI 0.4 flow chambers (ibidi, Martinsried, Germany) and transfected 24 hours later using jetPRIME reagent (Polyplus), as described above. Cell lines were obtained from the either commercial companies or from the repositories detailed in the key resources table and used as received, consistent with their established authentication. All cell lines used were confirmed to be mycoplasma-free.

METHOD DETAILS

Molecular cloning and mutagenesis

mVSP[25] was subcloned into both pEGFPC and pRFPC vectors using the BamH1 restriction sites. Basigin, embigin and neuroplastin were amplified from mouse brain cDNA and subsequently subcloned into both pEGFPN and pRFPN vectors using specific restriction

sites: XhoI /BamHI for basigin, HindIII/ApaI for embigin, and Xho1/Apa1 for neuroplastin. An external hemagglutinin (HA) epitope tag was introduced into the extracellular loop of mVSP at position 301 using insertional mutagenesis. Both ends of the epitope were flanked by PGG residues to enhance accessibility and flexibility of the extracellular HA tag, resulting in the sequence, which reads ^{301}**K**PGGYPYDVPDYAGGP**H**^{302}. VSP orthologs, Ci-VSP and Dr-VSP were subcloned into the pEGFPC and pEGFPN vectors, using the restriction sites BspEI /BamHI for pEGFPC, and EcoRI /ApaI for pEGFPN, respectively. m/ci-VSP and ci/m-VSP chimeras were generated using the overlap extension PCR method.[65] To create the m/ci-VSP chimera, the N-terminal region of mVSP, including amino acids from methionine 1 (M1) to glutamine 334 (Q334), was fused to the C-terminal cytoplasmic region of Ci-VSP, including amino acids from methionine 335 (M335) to isoleucine 576 (I576). For the ci/m-VSP chimera, the N-terminal cytoplasmic region of Ci-VSP, consisting of amino acids methionine 1 (M1) to arginine 119 (R119), was fused to a fragment of mouse VSP (mVSP) spanning amino acids isoleucine 216 (I216) to asparagine 664 (N664). Deletion mutagenesis was employed to generate a series of basigin mutant constructs. The ΔIgD1 variant was created by removing the first extracellular immunoglobulin (Ig) domain, corresponding to amino acids alanine 22 (A22) to valine 101 (V101). The ΔIgD2 construct lacks the second extracellular Ig domain, spanning lysine 112 (K112) to arginine 207 (R207). The ΔC-terminal variant was produced by deleting the intracellular C-terminal region of basigin, from glutamine 241 (Q241) to threonine 273 (T273). To introduce a Myc or flag tag at the C-terminus of basigin, PCR amplification was performed followed by subcloning the amplified product into the pcDNA3.1 vector using Xho1/BamH1 restriction sites. Similarly, *mVSP* was amplified using primers containing Xho1 restriction sites and subcloned into a pcDNA3.1 vector containing a 3xFLAG tag, ensuring that the tag is in frame with the C-terminus of mVSP. Both mVSP and basigin were subcloned into yeast two-hybrid vectors according to the manufacturer's recommended protocol using the Sfi1 restriction sites to ensure the insert is in-frame with the reporter cassette. Basigin$_{ERret}$ and embigin$_{ERret}$ constructs were generated using a strategy similar to the one employed for generating the neuroplastin$_{ERret}$ construct.[39] Point mutations were introduced using PfuUltra II Hotstart PCR Master Mix (Agilent Technologies, Santa Clara, US). All DNA constructs were confirmed by sequencing.

Split-ubiquitin membrane yeast two-hybrid assay

To identify proteins that interact with mVSP, we utilized the split-ubiquitin variant of the yeast-two-hybrid system (MoBiTec, Göttingen, Germany). This assay enables the use of full-length integral membrane proteins as baits, and it screens for interactions with both integral membrane proteins and membrane-associated proteins.[66–68] Briefly, the *Saccharomyces cerevisiae* reporter strain NMY51 was transformed with bait plasmid and the correct expression of the bait was verified by western blot using LexA monoclonal antibody (Santa Cruz Biotechnology). Verification of correct topology of the bait was performed using pAl-Alg5 and pDL2-Alg5 control preys, and the upper limit of selection stringency for screening was determined as SD -leu/-trp/-his/-ade (SD-LWHA) selection medium (Figures S1B–S1D). For screening, NMY51 yeast strain expressing the bait (mVSP) was transformed with a mouse brain cDNA library (MoBiTec). Positive clones were identified by following the manufacturer's protocols for the recovery of library plasmids and prey sequences. Protein-protein interaction was determined by growth on plates lacking the amino acids leucine, tryptophan, histidine, and adenine (-LWHA). Positive colonies were additionally confirmed using the second marker β-galactosidase. The nucleotide sequence of the positive clones was determined by sequencing, and the identity of the encoded putative interacting proteins was determined by a database search.

Co-immunoprecipitation

Two sets of experiments were carried out using lysates from HeLa cells. The cells were lysed using a buffer containing 50 mM Tris-HCl, pH 7.5, 150 mM NaCl, 1% Triton X-100, containing freshly added protease-inhibitor cocktail (SERVA). In the first set, lysates from HeLa cells expressing flag-tagged basigin and GFP-tagged mVSP were used. In the second set, lysates from HeLa cells expressing 3xflag-tagged mVSP and GFP-tagged basigin were used. Immunoprecipitations were performed using anti-FLAG M2 magnetic beads from Sigma, following the protocol provided by the manufacturer. The anti-FLAG M2 magnetic beads were coated with the lysates to facilitate the immunoprecipitation process. The antibody-coated beads were incubated with the cell lysates at 4°C for 12 hours under rotation. The beads coated with the antigen-antibody complex were washed extensively with 1 x PBS (four times), and the proteins on the beads were eluted by boiling at 72°C for 10 minutes in 2 x SDS sample loading buffer (20% v/v glycerol, 100 mM Tris, 130 mM DTT, 6.5% w/v SDS, 0.013% (w/v) bromphenol blue). Subsequently, the eluted proteins were separated using 10-12% SDS-PAGE under reducing conditions. The separated proteins were then transferred to a nitrocellulose membrane for further analysis. The membrane was probed with either a mouse anti-GFP antibody at a dilution of 1:1000 from Santa Cruz Biotechnology, Dallas, US or a monoclonal ANTI-FLAG® M2 antibody at a dilution of 1:1000 (Sigma-Aldrich). The membrane was washed and visualized with fluorescent secondary antibodies at a dilution of 1:5000 from Bio-Rad, Feldkirchen, Germany, and the immunoreactivity was detected using a ChemiDoc MP imaging system (Bio-Rad Feldkirchen, Germany).

Surface quantification assay in HeLa cells

Surface quantification of Basigin and its mutants in HeLa cells was carried out using an HRP-based chemiluminescence assay, as previously described.[69] Briefly, HeLa cells were transfected with the respective constructs using JetPrime (Polyplus). After 48 hours, the cells were fixed with 4 % PFA and incubated with a polyclonal anti-Basigin primary antibody (1:1000, R and D Systems) targeting

its extracellular domains, followed by a horseradish peroxidase (HRP)-conjugated secondary antibody (1:1000, Santa Cruz Biotechnology). Surface quantification was then measured by luminometry using an HRP luminogenic substrate (SuperSignal ELISA Femto solution, Thermo Scientific).

Confocal microscopy

HeLa, HEK or COS7 cells were analyzed 24-48 h after transfection using an upright LSM 710 - Axio Examiner Z1 microscope equipped with a W Plan/Apochromat 20x/1.0 DIC M27 75 mm water immersion objective and 100×/1.30 NA Oil UV objective (Zeiss, Jena, Germany). Red fluorescent protein (RFP) was excited at 561 nm with a DPSS 561-10 laser (Zeiss) and fluorescence emission was sampled at 582-754 nm. Green fluorescent protein (GFP) was excited at 488 nm with an argon laser and fluorescence emission was recorded at 493-597 nm.

Quantitative assessment of mVSP localization in the PM through membrane-to-cytosol ratio calculation

In order to determine the surface localization of mVSP at the PM, HeLa cells were co-transfected with GFP-tagged mVSP and RFP-tagged BSG. Cells were imaged 48 hours post-transfection using a ZEISS LSM 710 upright confocal microscope. Image analysis was performed with FIJI/ImageJ. For each cell, fluorescence intensity profiles were generated by drawing a line across the cell and plotting intensity (y-axis) versus distance (x-axis). PM localization was determined based on BSG-RFP fluorescence, as BSG is known to localize predominantly to the PM. The peak RFP fluorescence intensity along the line was taken as the PM intersection. Corresponding GFP-mVSP intensity values were extracted along the same profile. Subsequent quantitative analysis was performed using Microsoft Excel (Redmond, WA, USA). PM positions were identified by the maximum BSG-RFP signal (reference points R1 and R2, as shown in Figure S3). Corresponding mVSP fluorescence values at these points were considered as PM-localized signal (G1 and G2), while values between G1 and G2 were treated as cytosolic. The PM intensity (G1 and G2) was divided by the mean cytosolic intensity. A ratio greater than 1 indicated PM localization of mVSP, whereas a ratio less than 1 indicated cytosolic retention.

Assessment of VSP activity by total internal reflection microscopy

To assess the catalytic activity of VSP without relying on electrophysiological methods, we utilized ROMK2-Flp-In 293 cells,[47] that stably express the weak inward rectifier K^+ channel ROMK2 that effectively provides a constitutively high K^+ conductance. This conductance clamps the membrane potential (V_M) close to the K^+ equilibrium potential, thereby allowing for precise alteration of V_M by changing extracellular K^+ concentration (K^+_{ex}) in a temporally well-controlled manner.

Enzymatic activity against PI substrates in response to depolarized V_M was measured by monitoring membrane association of genetically encoded lipid biosensors specifically recognizing individual PI species by TIRF microscopy.[6,70]

TIRF experiments were done on a Dmi8 microscope (Leica, Wetzlar, Germany) equipped with an Infinity TIRF module (Leica), a HC PL APO 100x/1.47 oil objective (Leica) and a widefield laser (Leica). GFP and RFP fluorescence was excited at 488 nm and 561 nm, respectively, at a nominal penetration depth of 90 nm. Corresponding emission light passed GFP-T (505-555 nm) or DS-Red-T (590-650 nm) (Leica). Images were acquired at frame rates of 2 or 5 s with an ORCA-Flash4.0 C13440-20C camera (Hamamatsu photonics, Hamamatsu, Japan) controlled by LAS X software (Leica).

ROMK2-Flp-In 293 cells were seeded into glass bottom μ-slide VI 0.5 flow chambers (ibidi, Martinsried, Germany) and were co-transfected with GFP- or RFP-tagged phosphoinositide probes (PLCδ1-PH, tubbyCT, TAPP1-PH) and RFP- or GFP-tagged VSP constructs. Where appropriate, Myc-tagged BSG was co-transfected to promote membrane localization of mVSP. 48hrs after transfection, cells were analyzed by TIRF-M. μ-slides were mounted onto TIRF setup and individual flow chambers were perfused from a gravity-driven perfusion system. Chambers were continuously perfused with a solution containing either 2 mM (Figures 7A–7H) or 1.5 mM K^+_{ex} (Figures 7J–7N), and intermittently switched to higher K^+_{ex} for 1 minute intervals.

Solution composition was (in mM): X KCl, Y NaCl, 2 MgCl2, 1.3 CaCl2, 5.6 Glucose, 10 HEPES, adjusted to pH 7.4 with NaOH. For each KCl concentration (ranging between 1.5 and 150 mM), NaCl concentration was adjusted such that X+Y was 150 mM.

For experiments, individual cells with robust membrane localization of the respective VSP construct, as assessed by the fluorescence tag, were selected. Imaging was performed at room temperature (22°C–24°C).

TIRF microscopy data were analyzed using Fiji software by drawing a region of interest (ROI) within the cell and performing background subtraction using an ROI outside the cell. Mean fluorescence intensity of the ROI was calculated for each frame. Obtained data were exported to IgorPro (WaveMetrics) for further analysis. Time resolved fluorescence was normalized to signal intensity prior to each step in K^+_{ex} to yield normalized fluorescence intensity (F/F_0), which is presented plotted as a function of time. For quantification of voltage sensitivity, F/F_0 changes ($\Delta F/F_0$) resulting from application of the different K^+_{ex} concentrations were normalized to $\Delta F/F_0$ obtained at 150 mM K^+_{ex} for each recording (i.e. each cell).

Patch clamp electrophysiology

Whole-cell patch clamp experiments were performed on non-transfected ROMK2-Flp-In 293 cells. Membrane potential was continuously recorded in current clamp mode (at zero holding current) with an EPC 10 amplifier controlled by PatchMaster software (HEKA Elektronik, Lambrecht, Germany). Patch pipettes were pulled from 1mm OD borosilicate glass capillaries using a P-2000 laser puller (Sutter Instrument Company, Novato, CA, USA) to result in open pipette resistance of 2-3 MΩ after back-filling with intracellular solution containing (mM) 135 KCl, 0.1 $CaCl_2$, 3.5 $MgCl_2$, 5 HEPES, 5 EGTA, 2.5 Na_2ATP, adjusted to pH 7.3 (with KOH). Whole-cell series resistance (R_s) was below 10 MΩ. Cells were perfused through a local perfusion capillary from a gravity-driven perfusion system with

the same extracellular solution used for TIRF live-cell imaging. Recordings were done at room emperature (22°C–24°C) and recorded membrane potential was corrected for liquid junction potential (4.2 mV).

Structure predictions

The structure predictions were performed with AlphaFold-Multimer[42] version 2.3.1 and AlphaFold3.[43] In the AF-Multimer predictions, the maximum template release date was set to 2022-01-18. Five predictions per model resulted in 25 predictions per sequence. Only transmembrane regions of the proteins were considered, with mBasigin, mVSP, and Ci-VSP models covering residues 208–237, 196–344, and 101–249, respectively. Structures by AF3 were predicted by AlphaFold server resulting in five predictions per sequence. In the AF3 predictions, the models included both Ig and phosphatase domains and covered residues 22–240 (mBasigin), 191–664 (mVSP), and 101–576 (Ci-VSP). The N- and C-terminal parts of the sequences were trimmed, to avoid structural interference by disordered regions of a protein. In the contact analysis, a pair of residues was considered to be in contact if at least one pair of their atoms were within 5 A from each other.

QUANTIFICATION AND STATISTICAL ANALYSIS

Graphs and statistical analyses were carried out using either GraphPad Prism software (GraphPad Software, San Diego, CA, USA) or with Igor Pro (WaveMetrics). Data are reported as means ± SEM. Statistical significance was determined using an unpaired t-test or one-way ANOVA for more than two groups. For multiple comparisons to a single control condition, Dunnett's test was performed following ANOVA. In the figures, statistically significant differences to control values are marked by an asterisk (*$P < 0.05$, **$P < 0.01$, ***$P < 0.001$, ****$P < 0.0001$); ns indicates non-significant differences ($P > 0.05$). All statistical details can be found in the figure legends.

Bioinformatics

SMART (a Simple Modular Architecture Research Tool) and ELM (The eukaryotic linear motif) databases were used for predicting domains.